UNIVERSIDAD NACIONAL AUTÓNOMA DE MÉXICO

PROGRAMA DE POSGRADO EN ASTROFÍSICA

Instituto de Astronomía

HISTORIAS QUÍMICAS DE LAS GALAXIAS ESPIRALES DEL SUB-GRUPO LOCAL DE ANDRÓMEDA

PARA OPTAR POR EL GRADO DE
DOCTOR EN CIENCIAS (ASTRONOMÍA)

PRESENTA

FÁTIMA GUADALUPE ROBLES VALDEZ

TUTORA

DRA. MARÍA LETICIA CARIGI DELGADO

INSTITUTO DE ASTRONOMÍA

MÉXICO, D. F., ENERO, 2014

A César,

Por hacerme compañía durante este camino...

Solo hay una cosa que no se puede hacer con la química del Universo: Ignorarla
Fátima Robles Valdez

Agradecimientos

Agradezco a mi asesora de tesis, Leticia Carigi, un excelente ejemplo a seguir. Como tutora siempre estuvo dispuesta a compartir su conocimiento, y como amiga me tendió la mano en cada momento que lo necesité. Muchas gracias Leti.

A Manuel Peimbert, por su soporte en todo mi proceso académico y darme un espacio en su agenda, también por ser un magnífico colaborador en este trabajo.

A los sinodales: Dr. Juan Pablo Torres Papaqui, Dra. Elena Jiménez Bailon, Dr. Yalia Divakara Mayya, Dr. Manuel Peimbert Sierra y Dra. María Leticia Carigi Delgado, por dedicar parte de su tiempo a leer esta tesis, y por sus comentarios que ayudaron a mejorarla.

A mi mamá y mi hermano, que a pesar de la distancia puedo sentir que siempre están a mi lado, quienes en muchas ocasiones escogieron para si mismos caminos muy difíciles de andar para que mis pasos fueran más fáciles de dar. No encuentro palabras con las cuales pueda expresar mi enorme gratitud por su incondicional apoyo, ustedes son mi alma y mi corazón.

A mi hermoso hijo, que logra hacerme reír cada día, cuando menos lo espero, con sus tantas ocurrencias. Por sus preguntas inquietas que mantienen mi curiosidad despierta, por ser tan comprensivo a corta edad y darme la manita al paso de estos años, en tus ojos está mi Universo.

A Eduardo Ortiz, por los cafés, las idas al cine, los paseos, las visitas a las librerías, por las largas conversaciones... podría seguir haciendo una lista que se extendería a varias páginas, gracias por todo el espacio y el tiempo que compartes conmigo.

A Nancy Ávila, que apareció de último momento en mi estancia en el DF, y en poco tiempo se ganó un lugar especial en mi vida, estoy muy contenta de conocerte, eres una persona maravillosa.

A mis amigos, que compartieron sus esfuerzos, sus trotes y sus éxitos, son una parte primordial de mi desarrollo como estudiante y como persona, Ika, Ingrid, Regis, Jackie, Fabiola. A los que están lejos y nunca se les olvido escribirme hermosas cartas, Brenda, Sergio, Caro, y a quienes me hicieron soltar carcajadas con sus bromas Joel, Pancho, Alejandro...seguro se me escapan nombres, soy algo despistada, en fin, gracias a todos los compañeros de estas andanzas.

Al Instituto de Astronomía de la Universidad Nacional Autónoma de México, por brindarme un lugar tan agradable para desarrollarme como científico.

Al Consejo Nacional de Ciencia y Tecnología, CONACyT, por la beca otorgada durante mis estudios y al proyecto 129753-CONACyT.

Resumen General

En este proyecto de tesis se desarrollaron modelos de evolución química (CEMs) para las galaxias espirales del Triángulo y de Andrómeda, las cuales forman parte del Grupo Local. Estos modelos permiten estudiar la distribución espacial y temporal de los elementos químicos contenidos en el gas del medio interestelar de cada galaxia, así como los perfiles radiales de la masa de gas, la tasa de formación estelar y la masa estelar. Los CEMs fueron construidos para reproducir las mejores observaciones relacionadas con la química a tiempo presente, principalmente en los discos galácticos. Debido a que los ajustes de los modelos con las observaciones fueron de muy buena calidad, se infirieron propiedades de los procesos de formación galáctica y de formación estelar durante la vida de estas galaxias.

Básicamente los ingredientes con los que se construyeron los CEMs son: i) escenario de formación galáctico dentro-fuera, formación más eficiente y temprana hacia el centro de la galaxia que en su periferia; ii) función de masa inicial de Kroupa et al. (1993), con esta función los CEMs de la Vecindad Solar reproducen excelentemente las abundancias químicas observadas; iii) tasa de formación estelar que sigue la ley de Kennicutt-Schmidt, dada por: SFR = $\nu \mathrm{M}_{gas}^{1.4}$, con diferentes parametrizaciones de ν, que representa la eficiencia de formación estelar; iv) rendimientos químicos estelares, dependientes de la metalicidad y de la masa inicial de cada estrella formada, que representan la eficiencia de una estrella en producir nuevos elementos químicos y eyectarlos al medio interestelar.

A partir del CEM de la galaxia del Triángulo, se infirió que ésta se formó acorde a un escenario de formación estelar dentro-fuera suave para radios interiores ($r \leq 6$ kpc). Sin embargo, su formación estelar en las partes exteriores ($r > 6$ kpc) sigue un escenario fuera-dentro, debido a una eficiencia de formación estelar que disminuye en radios exteriores, de afuera hacia dentro, durante los últimos Gaños de evolución. Por lo tanto, esta galaxia de masa intermedia, en zonas internas, donde la masa bariónica es alta, presenta conductas de formación estelar semejantes

a las grandes espirales, mientras que en zonas externas, donde la masa bariónica es baja, presenta comportamientos de formación estelar semejantes a galaxias enanas.

A partir del CEM de la galaxia de Andrómeda, se infirió que la eficiencia de formación estelar es variable en el espacio, decreciente para $r < 8$ kpc, ligeramente plano para $8 < r$(kpc)< 11 y creciente para $r > 11$ kpc; para la mayor parte de la evolución de la galaxia ($t < 12.8$ Gaños). Por lo tanto el modelo predice tres pendientes en los gradientes químicos, conforme a las variaciones de la eficiencia en la SFR, las cuales estan en acuerdo con las abundancias observadas. El comportamiento radial de la eficiencia de formación estelar puede ser causado por diversas condiciones físicas en el gas del disco de Andrómeda, como la distribución y temperatura del gas molecular, procesos de turbulencia, entre otros. Hasta el momento, la causa y la evolución de la SFR sigue siendo un problema abierto en la astronomía.

Índice general

Capítulo 1

Introducción: Evolución Química de Galaxias Espirales

Las galaxias se forman a partir de acreción de gas principalmente conformado por hidrógeno y helio. Parte del gas acretado se transforma en estrellas, y estas enriquecen el gas de las galaxias con helio y elementos químicos más pesados que el helio.

La evolución química de galaxias espirales estudia los cambios en el espacio y el tiempo, de las abundancias químicas, y otras propiedades del gas y de las estrellas, presentes en el disco galáctico. Los modelos de evolución química tratan de reproducir, y por ende explicar, los procesos que ocurrieron en una galaxia o región de una galaxia, que nos den una interpretación física de los datos observacionales. Consecuentemente, buenos acuerdos entre lo predicho y lo observado permiten mejores inferencias de los procesos de formación y de evolución galáctica y estelar.

1.1. Restricciones Observacionales

Las restricciones observacionales son los datos obtenidos de las observaciones que permiten delimitar los parámetros libres de un modelo y por ende inferir la historia química del objeto de estudio.

Un CEM para una galaxia espiral debe reproducir, al menos, las siguientes tres distribuciones radiales: i) La masa de gas, $\mathrm{M}_{gas}(r)$ ii) La masa total bariónica, $\mathrm{M}_{tot}(r) = \mathrm{M}_{gas}(r) + \mathrm{M}_{estelar}(r)$ y iii) El gradiente de un elemento químico $\mathrm{X}_i(\mathrm{r})/H(\mathrm{r})$.

La M_{gas} incluye gas atómico y molecular de todos los elementos químicos (hidrógeno, helio y elementos pesados, Z). La $\mathrm{M}_{estelar}$ incluye estrellas vivas y

remanentes estelares, considerando que las estrellas muertas son el 13 % de las estrellas vivas (comunicación privada, L. Carigi y M. Peimbert).

Para los CEMs que presentamos, se ha considerado que el gradiente de oxígeno es el más importante, ya que el oxígeno puede representar más del 50 % de los metales, porcentaje que disminuye con la evolución. Las abundancias de O/H son tomadas de regiones H II y de estrellas gigantes y supergigantes, ambas asociadas a estrellas jóvenes y por lo tanto representan las abundancias químicas en el presente.

A fin de obtener un gradiente de O/H confiable y congruente, la abundancia gaseosa de O/H en cada region H II se ha corregido según las líneas usadas para su determinación y según la cantidad de oxígeno atrapado en granos de polvo (Peimbert & Peimbert 2010). Las abundacias gaseosas estimadas con líneas de excitación colisional son incrementadas por 0.23 dex (Esteban et al. 2009), debido a que estas líneas son sensibles a las variaciones de temperatura (Peimbert et al. 2007). Las abundancias gaseosas determinadas a partir de líneas de recombinación no requieren esta corrección, ya que son insensibles a las variaciones en la temperatura (Peimbert et al. 2007). Además, ambas abundancias gaseosas son aumentadas por 0.11 dex (Peimbert & Peimbert 2010), debido al polvo. En nuestros estudios, y otros trabajos anteriores, se ha notado que las abundancias químicas de regiones H II concuerdan con las abundancias químicas estelares, solo cuando las abundancias gaseosas de dichas regiones son corregidas como se ha indicado.

Los resultados de nuestros modelos se comparan con otras distribuciones radiales, como son: la tasa de formación estelar SFR(r), la masa de estrellas $M_{estelar}(r)$ y los gradientes de todos los elementos químicos observados en regiones H II y estrellas gigantes y super gigantes, $X_i(r)/H(r)$.

La calidad de los ajustes entre los datos observacionales y teóricos indicará la robustez de las deducciones hechas en base a los CEMs.

1.2. Modelos de Evolución Química, CEMs

Los CEMs estan basados en las ecuaciones estándar de evolución química, las cuales fueron escritas originalmente por Tinsley (1980), y son actualmente usadas por varios autores (por ejemplo: Matteucci 2001; Prantzos 2008; Pagel 2009). Los modelos de evolución química se construyen, ex profeso, para reproducir tres restricciones observacionales principales, los perfiles radiales en el disco galáctico de: la masa total bariónica, la masa de gas, y las abundancias de O/H. El resto de los perfiles radiales teóricos son consecuencia de los CEMs.

Un conjunto básico de ingredientes definen a los CEMs: i) el mecanismo de

formación de la galaxia, escenario dentro-fuera; ii) la tasa de formación estelar (SFR); iii) la función inicial de masa (IMF); iv) la matriz de rendimientos químicos estelares.

El escenario de formación galáctica dentro-fuera, dicta que la galaxia se forma de manera más temprana y eficiente en la parte interna que en la parte externa.

La SFR indica la cantidad de masa gaseosa que se convierte en estrellas por unidad de tiempo. Se utiliza la SFR parametrizada por Kennicutt-Schmidt (Kennicutt 1998), dada por: SFR = ν $M_{gas}^{1.4}$, donde ν representa la eficiencia de la formación estelar. La inferencia de ν se logra al ajustar el perfil de la masa de gas. Esta eficiencia, junto con el escenario de formación dentro-fuera, determinará la pendiente teórica del gradiente de O/H.

La IMF da el número de estrellas de cada masa que nacen en una generación estelar. La inferencia de la masa de la estrella más masiva de la IMF se obtiene al reproducir el valor absoluto del gradiente de O/H. Se utiliza la IMF de Kroupa et al. (1993), debido a que reproduce exitosamente las propiedades químicas en la Vecindad Solar.

Un rendimiento químico estelar, de un elemento en particular, es la fracción de una estrella de masa inicial, m_{ini}, convertida en el elemento estudiado y que es eyectada al medio interestelar (ISM) durante la evolución y muerte de la estrella. Los rendimientos son obtenidos de modelos de evolución estelar y dependen principalmente de la m_{ini}, de la metalicidad inicial de las estrellas y de la interacción con otra estrella.

Las estrellas aisladas de baja masa (m_{ini} <9M$\odot$) enriquecen químicamente al ISM durante una lenta pérdida de masa y durante la fase de nebulosa planetaria (Karakas et al. 2010). Son responsables, aproximadamente, de la mitad del enriquecimiento de He y del C, del 80 % del N y de la mitad de los elementos más pesados que el Fe. Las estrellas aisladas de alta masa (m_{ini} >9M$\odot$) enriquecen químicamente al ISM durante una rápida pérdida de masa y durante la fase de supernovas (Kobayashi et al. 2006), son responsables de la mitad del enriquecimiento de He y C, de la mayor parte de los elementos pesados, como O, Mg, Si, y de la mitad de los elementos más pesados que el Fe. Las estrellas binarias de baja masa que interactuan entre si son las progenitoras de las SNIa (Nomoto et al. 1997). Estas supernovas producen una considerable cantidad de Fe, y en menor cantidad Si y S, entre otros elementos. Las estrellas menos masivas (m_{ini} <0.8M$\odot$) no contribuyen al enriquecimiento químico por sus largos tiempos de vida, mayores que la edad del Universo.

1.3. Estructura de la Tesis

La tesis está estructurada de la siguiente manera: El capítulo 1, introduce a la investigación desarrollada durante mi tesis. El capítulo 2 muestra un resumen de mi proyecto y sus resultados. Los capítulos 3 y 4 presentan los artículos de los mejores CEMs que he construído para las galaxias del Triángulo y de Andrómeda, el primero publicado en MNRAS, 429, 2351, 2013, y el segundo enviado a la Revista Mexicana de Astronomía y Astrofísica.

Capítulo 2

Estudio de las galaxias del Triángulo y de Andrómeda

2.1. CEMs de las galaxias del Triángulo y de Andrómeda

En esta tesis investigué las abundancias químicas y otros observables de las galaxias espirales del Triángulo (M33) y de Andrómeda (M31), para así contar con un grupo de observaciones confiables que restringió de manera sólida los modelos. Construí un conjunto de más de 100 modelos de evolución química para cada galaxia, seleccioné el mejor conjunto de parámetros, físicamente sustentados, que ajustaron a las tres restricciones observacionales principales: los perfiles actuales de la masa total bariónica, la masa de gas y la abundancia de O/H en los discos galácticos.

Los mejores CEMs que construí, tanto de M33 como de M31, son más robustos que aquellos mostrados por otros autores en trabajos previos (ver secciones 3.4 y 4.2 de esta tesis), ya que presento una mayor cantidad de observables para comparar los resultados teóricos, y los CEMs ajustan las observaciones como ningún modelo anterior ha logrado ajustarlas. Dado los buenos ajustes de los CEMs que muestro en este trabajo, es posible inferir historias confiables de formación galáctica y formación estelar.

Para la construción de los CEMs he ensamblado un amplio arreglo de rendimientos químicos estelares en forma de matríz. Para ello utilicé las tablas de rendimientos de Karakas 2010, Kobayashi et al. 2006 y Nomoto et al. 1997, para estrellas de diferentes masas que enriquecen el medio interestelar en diferentes tiempos y con distintos elementos químicos (ver capítulo Introducción). Esta ma-

tríz es el componente fundamental del código; cuenta con 123 especies químicas (elementos e isótopos), de las cuales el modelo, junto con otras suposiciones, predice la conducta espacio-temporal de la abundancia de cada especie.

En los CEMs que presento en esta tesis se reportan las predicciones teóricas inferidas al ajustar las observaciones de las distribuciones radiales de: masa de gas, tasa de formación estelar, masa estelar y gradientes de varios elementos químicos, 11 elementos para M33 y 17 elementos para M31. Además, fue estudiado el enriqueciemiento de helio y oxígeno, dados los datos observacionales, para r = 4.5 kpc y r = 15 kpc, en M33 y M31, respectivamente.

Para que el conjunto de abundancias químicas observadas, con las cuales comparé los CEMs, fuese congruente, apliqué correcciones a las obtenidas a partir de regiones H II según el método de determinación utilizado. Para las abundancias calculadas utilizando líneas de excitación colisional, usé el factor t^2, al considerar variaciones en la temperatura en las regiones observadas (Peimbert & Peimbert 2010). Para estas abundancias y las abundancias obtenidas utilizando líneas de recombinación lineal, agregué la corrección por la cantidad del elemento químico estudiado dentro de granos de polvo (Peimbert et al. 2007). Al juntar las abundancias estelares con las de regiones H II concluí que ambas abundancias son acordes, si y solo si, las abundancias de regiones H II son corregidas por cambios de temperatura en el gas y por cierta cantidad de elementos químicos atrapados en polvo.

Para comparar los resultados de los modelos con valores consistentes de la masa de gas en el disco de cada galaxia, consideré el gas atómico y molecular de hidrógeno y además añadí la contribución por helio y elementos pesados, donde es tomado en cuenta el enriquecimiento de He y O de Carigi & Peimbert (2008), y que la metalicidad y el O/H del medio interestelar están escalados de igual manera que los respectivos valores solares (más detalles en 3.3.1).

2.2. Conclusiones Principales

A continuación muestro las conclusiones principales deducidas de los mejores CEMs que construí para M33 y para M31. En los capítulos 3 y 4 puede verse un conjunto más amplio de conclusiones para cada galaxia.

Las galaxias M31 y M33 se formaron bajo un escenario de formación galáctico dentro-fuera, con diferente escala de tiempo de formación para cada galaxia. Esto se infirió al reproducir el perfil radial de la masa de gas y el gradiente de O/H.

a) Para M33, se infirió un escenario de formación suave, formándose ligeramente más rápido la parte interna que la externa.

El comportamiento suave de la caída de material para la formación de M33 puede estar relacionado con su baja masa, considerablemente menor que el de las galaxias espirales mayores del Grupo Local (M31 y MW).

b) Para M31 se infirió un escenario de formación galáctico pronunciado, formándose mucho más rápido la parte interna que la externa.

El comportamiento pronunciado de la caída de material para la formación de M31 puede estar relacionado con su alta masa, siendo la galaxia espiral más masiva en el Grupo Local.

La posible correlación de la intensidad del escenario de formación galáctico dentro-fuera con la masa de las galaxias del Grupo Local serán estudiadas en trabajos futuros (ver sección 2.3)

ii) La eficiencia de la tasa de formacion estelar (ν = SFR/$M_{gas}^{1.4}$) depende del tiempo y del radio galactocéntrico de manera diferente para M31 y M33. Esto se infirió al reproducir el perfil radial de la masa de gas y el gradiente de O/H, ambas restricciones observacionales básicas.

a) Para M33 se infirió que para $r < 6$ kpc la eficiencia de formación estelar es constante en el tiempo y el espacio, mientras que para $r > 6$ kpc la eficiencia decrece a tiempos más tempranos y desde radios más externos. Esto significa que para $r < 6$ kpc la formación estelar es dentro-fuera, como la formación de la galaxia, debido a la acreción de gas; mientras que para $r > 6$ kpc la formación estelar es fuera-dentro, debido a la disminución de la eficiencia de la SFR desde fuera hacia dentro y desde el pasado al presente.

Una disminución de ν, como la inferida por este modelo, puede ser causada por una reducción en la densidad volumétrica de gas, aunque la densidad superficial permanezca constante o aumente (como lo observado en el disco de M33). La reducción de la densidad volumétrica puede originarse por deformaciones en el disco, estudiadas mediante simulaciones de N-cuerpos por Sanchéz-Blázquez et al. (2009). Este tipo de deformaciones han sido investigadas paticularmente para M33 por Corbelli & Schneider (1997), encontrando que M33 presenta el efecto de deformación o alabeo para $r > 7.5$ kpc.

b) Para M31 se infirió que para casi todo el tiempo de evolución de la galaxia (t <12.8 Gaños) y para todo r la eficiencia de formación estelar es variable con el radio. Para 12.8< t <13 Gaños y r >12 kpc, la ν se reduce casi a cero. Esto último con el fin de ajustar la SFR y la M_{gas} observadas.

La conducta de la eficiencia de la SFR variable con el radio y el tiempo puede ser causada por diferentes condiciones físicas en el gas del disco de M31, como la distribución del gas molecular, la temperatura de este gas, procesos de turbulencia, entre otras (Leroy et al. 2008; Zamora-Avilés & Semadeni 2013). Como es bien

sabido, los causantes, y por ende la evolución, de la SFR es un problema abierto en astronomía.

La reducción de la eficiencia en la SFR para radios externos y tiempos recientes puede deberse a un encuentro entre M31 y una de sus galaxias satélite, probablemente M31. Block et al. (2006), mediante simulaciones numéricas, explica la estructura anular observada en el disco de M31, entre 10 y 11 kpc, como resultado de un encuentro galáctico ocurrido hace aproximadamente 0.2 Gaños, y posiblemente el hecho de que el objeto que colisionó es considerablemente de menor masa que el disco de M31, produzca un efecto de reducción de la eficiencia en la SFR en radios externos al anillo formado, en lugar de un aumento, como se espera en un choque.

iii) Los gradientes quimicos predichos presentan de 2 a 3 pendientes en cada galaxia y los valores de esas pendientes son diferentes para M31 y M33. Esto es resultado del escenario de formación de las galaxias y la variación radial de la eficiencia de formación estelar.

En el campo de la evolución química, cada CEM es construído intentando reproducir, al menos, una restricción química básica. En esta tesis he tomado el gradiente de O/H en los discos galácticos, como principal restricción química, ya que el oxígeno representa más del 50 % de los metales (ver sección 1.1). Para ambas galaxias, los gradientes teóricos obtenidos al tiempo actual muestran muy buen acuerdo con las abundancias determinadas, tanto en regiones H II como en estrellas supergigantes.

a) Para M33, el gradiente de O/H predicho al tiempo actual presenta dos pendientes: en la parte más interna (0< r (kpc)<3) la pendiente es ligeramente negativa y en la parte externa (3< r (kpc)<9) la pendiente es marcadamente negativa. Para $r > 6$ kpc se requieren más datos observacionales, a fin de corroborar químicamente la formación estelar fuera-dentro en el disco externo.

b) Para M31, el gradiente de O/H predicho al tiempo actual presenta tres pendientes: en la parte interna (3< r (kpc)<8) la pendiente es ligeramente positiva, en la parte central (8< r (kpc)< 11) la pendiente es negativa, y en la parte externa (11< r (kpc)< 23) la pendiente es ligeramente negativa. Para $r > 11$ kpc se requieren más datos observacionales, para apoyar la predicción del aplanamiento del gradiente en la zona externa. Además, es recomendable obtener mejores estimaciones de las abundancias observadas para $r < 11$ kpc, ya que en esta región interna, los valores muestran un rango considerablemente amplio en sus errores.

2.3. Trabajo Futuro

Se pretende obtener correlaciones entre los resultados de modelos de evolución química (CEMs), robustos y consistentes, con las propiedades generales de galaxias espirales cercanas. A tal fin, se realizará una comparación química detallada entre las tres galaxias espirales del Grupo Local: Andrómeda (M31), Vía Láctea (MW) y Triángulo (M33).

Estas galaxias espirales muestran diferentes propiedades, como gradientes químicos, masa de gas, masa de estrellas y tamaños (radios galactocéntricos). La comparación entre los CEMs de estas 3 galaxias posiblemente nos permitirá determinar dependencias entre los escenarios de formación y mecanismos de evolución galácticos con las características principales de las galaxias espirales.

Debido a que ya contamos con CEMs para la espiral mas masiva (M31) y la menos masiva (M33), produciremos un modelo de evolución química para la galaxia de masa intermedia (MW). Este modelo se generará usando el mismo código y bajo ingredientes semejantes a los presentados en esta tesis.

Con este estudio esperamos aportar importantes deducciones a la astronomía extragaláctica y a la cosmología.

Bibliografía

Block D., Bournaud F., Combes F., Groess R., Barmby P., Ashby M., Fazio G., Pahre M., Willner S., 2006, Nature, 443, 832

Carigi L., Peimbert M., 2008, RMxAA, 44, 341

Corbelli E., Schneider E., 1997, ApJ, 479, 244

Esteban C., Bresolin F., Peimbert M., García-Rojas J., Peimbert A., Mesa-Delgado A., 2009, ApJ, 700, 654 (E09)

Karakas A., 2010, MNRAS, 403, 1413

Kennicutt A., 1998, ApJ, 498, 541

Kobayashi C., Karakas A., Umeda H., 2011, MNRAS, 414, 3231

Kroupa P., Tout C., Gilmore G., 1993, MNRAS, 262, 545

Leroy A., Walter F., Brinks E., Bigiel F., de Blok W., Madore B., Thornley M., 2008, AJ, 136, 2782

Matteucci F., 2001, Astrophysics and Space Science Library, Vol. 253, The Chemical Evolution of the Galaxy (Dordrecht:Kluwer),293

Nomoto K., Iwamoto N., Nakasato N., Thielemann F., Brachwitz F., Tsujimoto T., Kubo Y., Kishimotp N.,1997, NuPha, 621, 467

Pagel B., 2009, Nucleosynthesis and Chemical Evolution of Galaxies (Cambridge: Cambridge Univ. Press)

Peimbert M., Luridiana V., Peimbert A., 2007, ApJ, 666, 636

Peimbert A., Peimbert M., 2010, ApJ, 724, 791 (PP10)

Prantzos N., 2008, EAS Publications Series, 32, 311 (arXiv:0709.0833)

Sánchez-Blázquez P., Courty S., Gibson B., Brook C., 2009, MNRAS, 398, 591S

Tinsley B., 1980, Fundam. Cosmic Phys., 5, 287

Zamora-Avilés M., Vázquez-Semadeni E., 2013, submitted ApJ

Capítulo 3

Outside-in stellar formation in the spiral galaxy M33?

3.1. Abstract

We present and discuss results from chemical evolution models for M33. For our models we adopt a galactic formation with an inside-out scenario. The models are built to reproduce three observational constraints of the M33 disk: the radial distributions of the total baryonic mass, the gas mass, and the O/H abundance. From observations, we find that the total baryonic mass profile in M33 has a double exponential behavior, decreasing exponentially for $r \leq 6$ kpc, and increasing lightly for $r > 6$ kpc due to the increase of the gas mass surface density. To adopt a concordant set of stellar and H II regions O/H values, we had to correct the latter for the effect of temperature variations and O dust depletion. Our best model shows a good agreement with the observed radial distributions of: the SFR, the stellar mass, C/H, N/H, Ne/H, Mg/H, Si/H, P/H, S/H, Ar/H, Fe/H, and Z. According to our model, the star formation efficiency is constant in time and space for $r \leq 6$ kpc, but the SFR efficiency decreases with time and galactocentric distance for $r > 6$ kpc. The reduction of the SFR efficiency occurs earlier at higher r. While the galaxy follows the inside-out formation scenario for all r, the stars follow the inside-out scenario only up to $r = 6$ kpc, but for $r > 6$ kpc the stars follow an outside-in formation. The stellar formation histories inferred for each r imply that the average age of the stars for $r > 6$ increases with r.

3.2. Introduction

The Triangulum galaxy, or M33, is the third spiral galaxy in size within the Local Group, after the galaxy of Andromeda and the Milky Way. M33 is an Sc late-type galaxy of low-luminosity, about 20 times lower than that of the Milky Way. It does not present a bulge or a bar (Regan & Vogel 1994), and it is located at a distance of 840 kpc (Freedman et al. 1991). M33 has a deprojected semi-major axis of $\sim$ 9 kpc (Gil de Paz et al. 2007) and its baryonic mass is about one tenth of that of the Milky Way (Corbelli 2003).

It is important to study M33 because it is intermediate in mass between those galaxies in the Local Group that can be explained as formed by the inside-out scenario (M31 and the MW), and the small mass galaxies of the Local Group that are formed in an outside-in scenario (Hidalgo et al. 2011, Monelli et al. 2011).

The objective of this work is to study the evolution of M33 using chemical evolution models (CEMs) to infer the history of the chemical abundances of the gas content in the disk. We have recent observational data of the surface density of M_{gas} (Gratier et al. 2010), which shows a double exponential profile: a decreasing one for $r \leq 6$ with and a slightly increasing one for $r > 6$ kpc. We present more reliable values of chemical abundances, values consistent with H II regions and stars. Thanks to the recent increase in the quality of the data, we can infer a reliable chemical history of M33.

There are many models of M33 present in the literature, but they have not been able to explain all the relevant observational data. In particular we want to fit the properties of the central part of the inner disk, and of the outer disk simultaneously.

Throughout this paper we adopt the usual notation X, Y, and Z to represent the hydrogen, helium, and heavy elements abundances by mass, while the abundances by number are represented without italics. In §3.3 we describe the observational constraints used in this article. In §3.4 we review previous CEMs of M33. In §3.5 we present the features of our chemical evolution models. In §3.6 we present the main results of our models. In §3.7 we discuss our most interesting outcome within the framework of the Local Group . The conclusions are presented in §3.8.

3.3. Observational constraints

In the present work, the chemical evolution models were built to reproduce three main observational constraints of the M33 disk: the radial distributions of the total baryonic mass, the gas mass, and the oxygen abundance, which are shown in Figures 3.1 and 3.2. The chemical evolution models were tested with other

observational constraints of the M33 disk, such as the radial distributions of: the star formation rate, the stellar mass, the chemical abundances of nine elements and the metallicity, which are shown in Figures 3.3, 3.4, and 3.5. Moreover, the models were built to reproduce the average abundance of iron in the M33 halo, considering the value $\langle[Fe/H]\rangle$ = -1.24, estimated for halo stars by Brooks et al. (2004). In this section, we describe the observations used to constrain the models as a function of the galactocentric distance, r, hereafter in kpc units.

3.3.1. Radial distribution of the gas mass surface density, $M_{gas}(r)$

$M_{gas}(r)$ represents the atomic and molecular gas that contains all the chemical elements in the disk of M33: X, Y, and Z; i.e. $M_{gas}(r) = M_X(r) + M_Y(r) + M_Z(r)$. In Figure 1 we show the $M_{gas}(r)$, as filled black circles, which includes the atomic and molecular components of X, Y, and Z.

To obtain $M_X(r)$ we use the updated surface density of hydrogen azimuthally averaged and corrected by the inclination angle by Gratier et al. (2010) from 0.5 to 8.5 kpc.

We added atomic and molecular hydrogen, the sum of both components shows an increase at $r > 6$ kpc, consequently $M_X(r)$ presents a double exponential profile (see Figure 8 by Gratier et al. 2010, and Figure 4 by Verley et al. 2009). In this context, Corbelli & Schneider (1997) observed the distribution of HI in the M33 disc, and found that the gas disk is deformed for $r > 7.5$ kpc, due to warp effects.

Since the helium mass fraction and heavy elements content were not included in the data by Gratier et al. 2010 (private communication, Gratier 2010), we computed $M_Y(r)$ and $M_Z(r)$ from the following relations:

i) The definition of abundance of an element by mass. Specifically: $M_Y(r)/M_X(r) = Y(r)/X(r)$ and $M_Z(r)/M_X(r) = Z(r)/X(r)$.

ii) The normalization of the chemical abundances by mass: $X(r) = 1 - Y(r) - Z(r)$.

iii) The $Y(r)$ and $O(r)$ enrichment by Carigi & Peimbert (2008): $Y(r) = 0.2477 + 3.3O(r)$.

iv) The transformation of O/X (by mass) to O/H (by number): $O(r)/X(r) = 16$ (O/H)(r).

v) The O/H gradient determined in this paper (see eq. 3.8): (O/H)(r)= $10^{-0.038r-3.253}$.

vi) The Z value in the interstellar medium (ISM) is proportional to the O/H ratio, like in the Sun: $Z(r)/(O/H)(r) = Z_\odot/(O/H)_\odot$.

vii) The protosolar values of $Z_\odot$ and $12 + \log(O/H)_\odot$ by Asplund et al. (2009), which are 0.0142 and 8.73 dex, respectively.

The contributions of Y and Z increase the gas mass surface density by a factor of 1.3 approximately, relative to X.

3.3.2. Radial distribution of the total stellar mass surface density, $M_{stars}(r)$

We show in Figure 3.1, as filled red triangles, the radial distribution of the total stellar mass used to restrict our models.

We took the radial distribution of mass surface density of living stars, $M_{starL}(r)$, from the profile of the stellar disk surface density from Figure 7 by Corbelli (2003), given by the expression:

$$M_{starL}(r) = 405e^{(-r/1.28kpc)}. \tag{3.1}$$

Recently, Saburova & Zasov (2012) determined a radial profile of the mass surface density of living stars, which is very similar to that by Corbelli (2003). In addition, we took into account the contribution to the stellar mass due to the stellar remnants, $M_{starR}(r)$, with a value equal to the 13 % of the living stellar mass, according to that computed in the Galaxy by Carigi & Peimbert (2011), thus:

$$M_{stars}(r) = M_{starL}(r) + M_{starR}(r) = 458e^{(-r/1.28kpc)}. \tag{3.2}$$

The observational profile present a single exponential profile.

3.3.3. Radial distribution of the total baryonic mass surface density, $M_{tot}(r)$

The total baryonic mass, $M_{tot}(r)$, shown in Figure 3.1, as filled cyan squares, is the sum of the gas mass and the stellar mass: $M_{tot}(r) = M_{gas}(r) + M_{stars}(r)$. The radial distribution of the total mass shows a double exponential profile: $M_{tot}(r)$ decays exponentially for $r \leq 6$ kpc and increases slightly for $r > 6$ kpc. Thus, the total mass of the M33 disk is given by:

$$M_{tot}(r) = 460e^{(-r/1.56kpc)}, \qquad for \qquad r \leq 6kpc.$$

$$\mathrm{M}_{tot}(r) = 9.33e^{(+r/125kpc)}, \qquad for \qquad r > 6kpc. \tag{3.3}$$

Error bars of the data are smaller than the size of the symbols, consequently the behavior of the profile is statistically reliable.

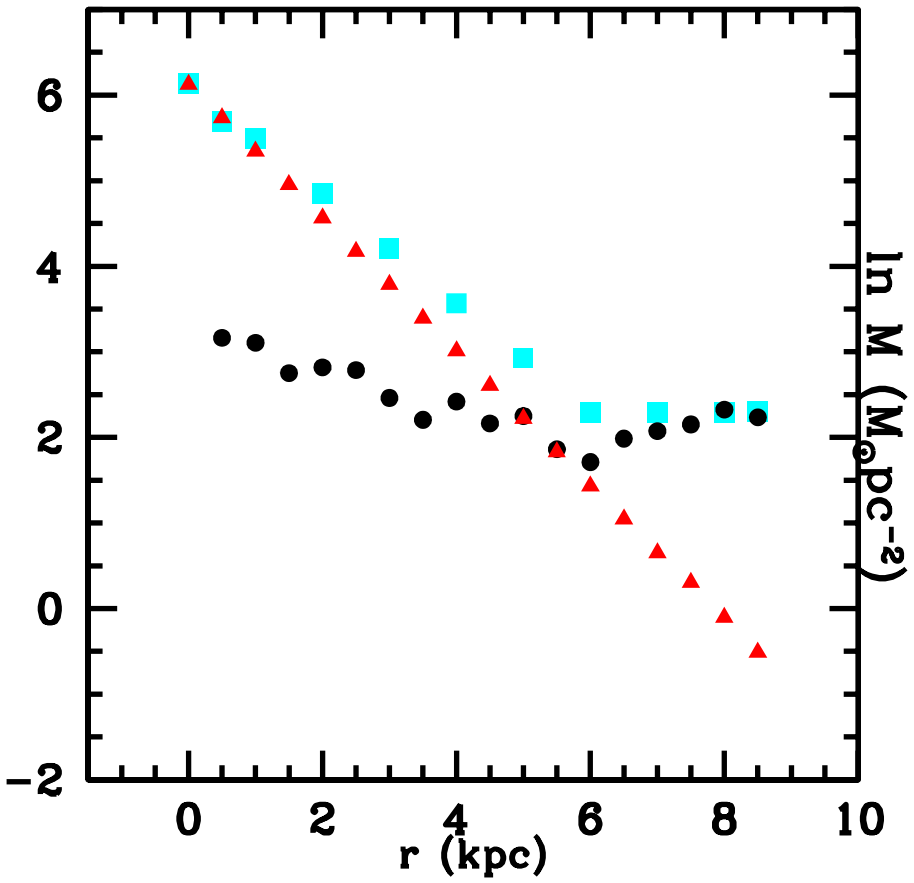

Figura 3.1: Radial distributions at the present time of: a) the gas mass (filled black circles): atomic and molecular hydrogen by Gratier et al. (2010) including the helium and heavy elements contribution, b) the total stellar mass (filled red triangles): living stellar mass by Corbelli (2003) plus stellar remnants mass according to Carigi & Peimbert (2011), c) the total baryonic mass (filled cyan squares). See sections 3.3.1, 3.3.2, and 3.3.3. The error bars are smaller than the size of symbols.

3.3.4. Radial distribution of the star formation rate, $SFR(r)$

M33 is a galaxy with an active star formation at the present time, as is shown by the large sample of H II regions and O-B stars.

In order to constrain the chemical evolution models, we considered the radial distributions of the star formation rate obtained by Verley et al. (2009). They calculate the transformation of H_α and far ultraviolet (FUV) luminosities, which have been corrected by dust extinction, using a stellar population synthesis model with continuous star formation, and they obtain that:

$$SFR(H_\alpha)[M_\odot yr^{-1}] = 8.3 \times 10^{-42} L(H_\alpha)[erg\ s^{-1}]). \quad (3.4)$$

$$SFR(FUV)[M_\odot yr^{-1}] = 8.8 \times 10^{-44} L(FUV)[erg\ s^{-1}]). \quad (3.5)$$

Verley et al. (2009) also computed the conversion of far infrared luminosity (FIR) to SFR. The FIR luminosity is less affected by dust extinction than the H_α and FUV luminosities, however the amount of re-radiation and the stars that heat the dusty environment have to be taken into account. Verley et al. choose the extinction corrected FUV as a reference and derive the conversion factor for the FIR waveband, obtaining:

$$SFR(FIR)[M_\odot yr^{-1}] = 13 \times 10^{-44} L(FIR)[erg\ s^{-1}]). \quad (3.6)$$

3.3.5. Chemical abundances

There are several studies on the chemical abundances of H II regions and O-B stars in M33, which well represent the present-time chemistry in the gas. We considered as observational constraint the O/H values from: H II regions by several authors (see below) and B supergiants by Urbaneja et al. (2005). The data used to built the chemical evolution models in this work have been corrected by the t^2 factor and dust depletion. Also we tested our models with other chemical abundances.

Rosolowsky & Simon (2008), using collisional excitation lines (CELs), obtained the O/H abundances in 61 H II regions. Since CELs are sensitive to temperature changes in the H II regions, these O/H values were corrected using the discrepancy factor, known as the t^2 factor (Peimbert et al. 2007). It is also necessary to add the dust-phase to the gas-phase component of the O/H values, due to the amount of oxygen atoms trapped in dust grains (Peimbert & Peimbert 2010, PP10). Therefore, O/H values by Rosolowsky & Simon (2008) were increased by 0.23 dex (Esteban et al. 2009, E09) and 0.11 dex (PP10) due to temperature

variations and oxygen embedded in dust grains, respectively.

E09, using recombination lines (RLs) obtained the C/H, N/H, O/H, Ne/H, Ar/H and Fe/H abundances in two H II regions: NGC 595 and NGC 604, not included in the sample of Rosolowsky & Simon (2008). The RLs are not sensitive to temperature variations, thus those abundances were not corrected by the t^2 factor. We corrected the C/H, O/H, and Fe/H abundances by dust depletion, increasing the gaseous values by 0.10 dex, 0.11 dex, and 1.00 dex, respectively (PP10, E09, Mesa-Delgado et al. 2009). The N/H abundances by E09 were not increased by dust depletion. Since neon and argon are noble gases they are not expected to be embedded in dust grains.

We also considered the O/H ratios determined by Magrini et al. (2010), in 33 H II regions. They used CELs to obtain these abundances, so their values were increased by 0.23 dex (E09) and 0.11 dex (PP10) by the t^2 factor and dust depletion, respectively. In addition, we used the S/H and Ar/H values computed by Magrini et al. (2007b) in 14 H II regions. Since those abundances were determined from CELs, we corrected them by the t^2 factor, adding 0.21 dex to the S/H values, and 0.24 dex to Ar/H values (E09). The S/H abundances by Magrini et al. (2007b) were not increased by dust depletion. As we mentioned previously, Ar atoms are not embedded in dust grains.

Recombination lines have been used by Bresolin (2011) to determine the O/H abundances in 25 H II regions, but we consider only two of these regions, since the rest of the sample is common to the sample of Rosolowsky & Simon (2008). The O/H ratios by Bresolin were increased by the t^2 factor and by dust depletion for 0.23 dex (E09) and 0.11 dex (PP10), respectively.

We used the Ne/H ratios by Willner & Nelson-Patel (2002) obtained from CELs in 25 H II regions. Therefore we corrected the data by the t^2 factor, adding 0.26 dex (E09), but not for dust depletion, due to the Ne is a noble gas.

Lebouteiller et al. (2006) derived the P/H abundance in the H II region NGC 604 from CELs. The P/H value was not corrected by either the t^2 factor or dust depletion.

The abundances obtained from O, B, and A stars correspond to the present day abundances in the ISM, since these stars have short lifetimes. We use the O/H, C/H, N/H, Mg/H and Si/H abundances estimated by Urbaneja et al. (2005) in 11 B supergiants. Instead of using the Z data by Urbaneja et al., we computed the Z values from the following equation:

$$Z_{stars}/Z_{\odot} = \frac{(C + N + O + Mg + Si)_{stars}}{(C + N + O + Mg + Si)_{\odot}}. \tag{3.7}$$

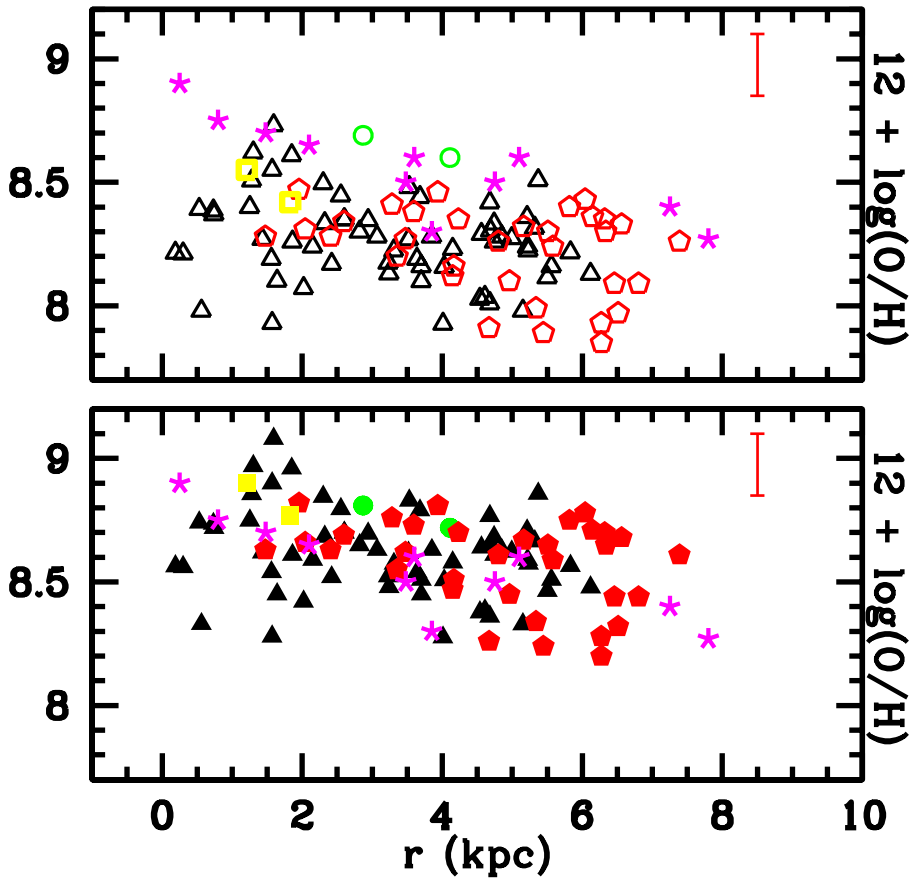

Figura 3.2: Observed radial distribution at present time of O/H ratios. Top panel: a) gaseous values from H II regions by Rosolowsky & Simon (2008) (empty black triangles), by Esteban et al. (2009) (empty green circles), by Bresolin (2011) (empty yellow squares), and by Magrini et al. (2010) (empty red pentagons), without correction by the t^2 factor and dust depletion. b) Stellar values from B supergiants by Urbaneja et al. (2005) (magenta asterisks). Bottom panel: a) gaseous values shown in top panel but now filled symbols, corrected by the t^2 factor and dust depletion. b) Stellar values as top panel. See section 3.3.5. The vertical red line represent the average error.

adopting the stellar abundances determined by Urbaneja et al. and the protosolar abundances by Asplund et al. (2009). The stellar values do not require corrections by either the t^2 factor, or by dust depletion.

In the top panel of Figure 3.2 we show the O/H gaseous values by: Rosolowsky & Simon (2008), E09, Bresolin (2011), and Magrini et al. (2010), without correction by the t^2 factor and dust depletion. In the bottom panel we show these O/H gaseous values corrected by the t^2 factor and dust depletion. Moreover, we plot the stellar O/H abundances by Urbaneja et al. (2005). It is remarkable that the average of the corrected O/H ratios from H II regions is similar to the O/H ratios from B stars. When the gaseous values are not corrected, the stellar abundances are higher, by ~ 0.3 dex.

Considering all the O/H gaseous values corrected by the t^2 factor and dust depletion, and the O/H stellar values, we obtain, using least-squares fit, the oxygen gradient as:

$$12 + log(O/H) = -(0.038 \pm 0.008)r + (8.747 \pm 0.035). \quad (3.8)$$

We also present abundances for 9 chemical elements and $Z/Z_{\odot}$ from H II regions (only the corrected ones) and B stars. See section 3.6.1 for additional details.

Moreover, in order to constrain the efficiency of the star formation rate in the halo, we used the mean abundance of iron, $\langle[Fe/H]\rangle$ = -1.24, estimated by Brooks et al. (2004). They obtained I and V photometry of the halo stars of M33, and constructed an I vs. $V - I$ diagram to derive the metallicity distribution function by interpolating between evolutionary tracks of red giant branch models. The value estimated by Brooks et al. is similar to $\langle[Fe/H]\rangle$ = -1.27, obtained from halo globular clusters by Sarajedini et al. (2000).

Also we compared the predicted ΔY and ΔO values with those observed in the H II region NGC 604. Then, we considered the He/H ratio obtained by Esteban et al. (2002), and the O/H ratio determined by E09. See section 3.6.2 for additional details.

3.4. Previous chemical evolution models for M33

In this section we discuss some chemical evolution models, CEMs, for M33 published in the literature. Previous models were built to reproduce or compare with: i) gas mass distribution that decays with r, even for $r > 6$ kpc and ii) O/H gaseous values without considering the t^2 factor and the correction by dust.

Mollá, Ferrini & Díaz (1996), Mollá, Ferrini & Díaz (1997), and Mollá &

Díaz (2005) presented a grid of CEMs and compared their results with several galaxies, including M33. In these three articles the CEMs were developed under the *SFR* prescription by Ferrini et al. (1992). This *SFR* is a product of the processes of conversion of diffuse gas into clouds and the collapse of these clouds to form stars. Also they used the initial mass function, IMF, by Ferrini et al. (1990), which is similar to that obtained by Kroupa (2001). Mollá and collaborators reproduced reasonably well the O/H abundances in comparing with the observations by Kwitter & Aller (1981) and Vílchez et al. (1988), but they failed to reproduce the $M_{gas}(r)$.

Magrini et al. (2007a) used a generalization of the multi-phase model by Ferrini et al. (1992). Their best model assumes an infall rate on the disk almost constant in time, a *SFR* prescription as Mollá & Díaz (2005) and a two power law IMF, analogous to the IMF by Kroupa, Tout & Gilmore (1993). This model presents a reasonable fit with the O/H abundances from H II regions (Kwitter & Aller 1981, Vílchez et al. 1988, Crockett et al. 2006, and Magrini et al. 2007b). Their predicted M_{gas} does not agree with the data by Corbelli (2003).

Barker & Sarajedini (2008) built a CEM under the instantaneous recycling approximation. They adopted the IMF by Kroupa, Tout & Gilmore (1993) and used a parametrization of the *SFR* according to the Kennicutt-Schmidt law (Kennicutt 1998) with a star formation efficiency constant in space and time. They compared the predicted oxygen gradient with the observed one from H II regions and A-B supergiants compiled by Magrini et al. (2007b). They obtained O/H values higher than the observed ones by 0.3 dex. Their predicted $M_{gas}(r)$ is considerably less than that observed.

Magrini et al. (2010) added to the observational constraints of their previous paper, a new sample of H II regions observed by themselves. Their new CEM is very similar to that built by Magrini et al. (2007a), but now they adopt the IMF by Ferrini, Penco & Palla (1990). Their model continue without reproducing the distribution of gas mass by Corbelli (2003) in the central region ($r < 1$ kpc) and in the outskirts ($r > 6$ kpc) of the galactic disk.

Marcon-Uchida, Matteucci & Costa (2010) built a CEM only for the M33 disk based on a version of the MW model by Chiappini, Matteucci & Romano (2001). They adopt the IMF by Kroupa, Tout & Gilmore (1993) and use a Kennicutt-Schmidt *SFR* with a low star formation efficiency and different thresholds in the gas density for the star formation. The predicted O/H abundances are overestimated for more than 0.25 dex compare to the observed values from H II regions. Moreover for $r < 4$ their model fails to reproduce the distribution of gas mass by Corbelli (2003) and Boissier, Gil de Paz & Boselli (2007), diverging completely

in the inner zone of the disk.

Kang et al. (2012) constructed a CEM under the instantaneous recycling approximation. They used the IMF by Chabrier (2003) and adopted a *SFR* law correlated with the mass surface density of molecular gas. The predicted O/H fits well the abundances obtained from H II regions, but its absolute value is lower than that determined from B supergiants, since they assume neither dust depletion, nor a t^2 factor . They reproduced well the observational gas mass for $r < 7$ kpc.

Since the previous CEMs cannot explain the main observational constraints for some regions of the disk and nowadays there are more precise observations, we have built new chemical evolution models for M33.

3.5. Chemical evolution models, CEMs

The CEMs of M33 are based on the standard chemical evolution equations, which were originally written by Tinsley (1980) and are currently used by several authors (e.g. Matteucci 2001, Prantzos 2008, and Pagel 2009). The models have been built to reproduce $M_{tot}(r)$, $M_{gas}(r)$, and O/H(r) (see section 3.3). We describe in detail the characteristics of the models below:

i) Halo and disk are projected onto a single disk of negligible width assuming azimuthal symmetry, therefore all functions depend only on the galactocentric distance r and time t. The single disk is a series of independent concentric rings (1 kpc wide) ranging from 0 to 9 kpc.

ii) M33 was formed in an inside-out scenario with a double-infall of primordial abundances: $Y_p = 0.2477$ and $Z = 0.00$ (Peimbert et al. 2007). The adopted double-infall rate is similar to that presented by Chiappini, Matteucci & Gratton (1997), and is given by $IR(r,t) = A(r)e^{-t/\tau_h} + B(r)e^{-(t-1Gyr)/\tau_d}$, where the halo formation occurs during the first Gyr with a timescale $\tau_h = 0.5$ Gyr (Carigi & Peimbert 2011), and the disk formation takes place from 1 Gyr until 13 Gyr (the age of the model), with a radial increasing timescale $\tau_d = (0.9r + 5)$ Gyr.

The variables $A(r)$ and $B(r)$ are chosen to reproduce the radial distribution of the total baryonic mass at the present-time in the disk component, $M_{tot}(r)$. We also considered that the distributions of disk and halo mass match the disk and halo components of the Solar Neighborhood, $M_{halo}/M_{disk} = 0.25$ (Carigi & Peimbert 2011). Since $M_{tot(r)}$ presents a double exponential profile, this is reflected in the infall rate, taking each one of these variables, $A(r)$ and $B(r)$, two values ,Äã,Äãdepending on the galactocentric radius: $A(r) = 92e^{-(r/1.56kpc)}$ and $B(r) = 368e^{-(r/1.56kpc)}$ for $r \leq 6$ kpc, and $A(r) = 1.8e^{+(r/125kpc)}$ and $B(r) = 7.5e^{+(r/125kpc)}$ for $r > 6$ kpc.

iii) The SFR was parametrized as the Kennicutt-Schmidt Law (Kennicutt 1998): $SFR(r,t) = \nu M_{gas}(r,t)^{1.4}$, where ν is the star formation efficiency obtained by adjusting the current gas mass radial distribution. In order to match the $\langle[Fe/H]\rangle$ shown in halo stars (see section 3.3.5) we assumed a ν value 5 times higher during the halo formation than that adopted for the disk.

iv) The models assume the initial mass function by Kroupa, Tout & Gilmore (1993), since the CEMs that considered this IMF reproduce the chemical properties of the Milky Way disk and of the Solar Neighborhood (Carigi & Peimbert 2011). In this work, we considered the mass range from 0.08 $M_\odot$ to an upper mass, m_{up}, where m_{up} = 50 $M_\odot$ was chosen to reproduce the current O/H gradient.

v) The models use an array of stellar yields for low and intermediate mass stars, LIMS ($0.08 \leq m/M_\odot \leq 8$), and for massive stars, MS ($8 < m/M_\odot \leq m_{up}$). All these yields depend on the initial metallicity and initial mass of the stars. In order to generate the complete matrix, we interpolated linearly the yields by mass and metallicity, and we extrapolated them, when necessary, by adopting the last available value. The set of yields includes:

a) For stars with masses from 13 to 40 $M_\odot$ and with Z = 0.0, 0.001, 0.004, and 0.02, we adopted the yields by Kobayashi et al. (2006). In the cases of Z = 0.008 and 0.02, we added to the yields by Kobayashi et al. an average of the stellar winds yields of intermediate mass loss rate for He, C, N and O, obtained by Maeder (1992) and Hirshi, Meynet & Maeder (2005), following the suggestion by Carigi & Peimbert (2011). For Z = 0, we increased the yields by Kobayashi et al. adding to them the rotation yields for He, C, N, and O, estimated by Hirshi (2007), that modification was based on the results by Kobayashi, Karakas & Umeda (2011).

b) For star with masses from 1 to 6 $M_\odot$ and with Z= 0.0001, 0.004, 0.008 and 0.02, we used the yields by Karakas (2010).

c) For binary stars, with total mass between 3 and 16 $M_\odot$, we adopted the yields by Nomoto et al. (1997) in the SNe Ia formulation by Greggio & Renzini (1983). We used the variable A_{bin} = 0.05 as the fraction of binary stars that are progenitors of SNe Ia. This A_{bin} value is chosen in order to reproduce the current Fe/H gradient.

vi) The stellar lifetimes were taken from Romano et al. (2005). These lifetimes are dependent on the initial stellar mass, but independent of initial stellar metallicity.

vii) We do not include radial flows of gas or stars. The loss of gas and stars from the galaxy to the intergalactic medium was not considered.

3.6. Results and discussion

We computed two chemical evolution models, CEM1 and CEM2, whose common characteristics were presented in the section 3.5. These two models are identical for $r < 6$ kpc and the only difference between them is the adopted values of the star formation efficiency, ν, for $r > 6$ kpc.

3.6.1. Radial distributions of M_{gas}, M_{stars}, SFR, and Chemical abundances

CEM with constant ν

CEM1 was built assuming a constant ν for $0 < r(kpc) < 9$ and for any time. First, we analyze the CEM1 results for $r \leq 6$ kpc, and then for $r > 6$ kpc.

For $r \leq 6$ kpc CEM1 reproduces very well the present time main observational constraints: the $M_{gas}(r)$ and O/H(r) (see Figure 3.3), according to inside-out galaxy formation scenario. With a given infall, the behavior of M_{gas} depends on the chosen SFR and consequently on its ν. To reproduce M_{gas}, we obtain $\nu = 0.02(M_{\odot}pc)^{-0.4}Gyr^{-1}$. Then, the oxygen abundance depends on the chosen IMF and its m_{up}. To reproduce the absolute value of O/H(r), we obtain $m_{up} = 50M_{\odot}$.

Moreover the predicted $SFR(r)$ and $M_{stars}(r)$ show very good fits with observations, see Figure 3.4. Both decrease with radius, similarly to the $M_{gas}(r)$, because M_{stars} is a time-accumulative process due to the SFR and the SFR is proportional to the M_{gas}.

Also the inferred radial distributions of chemical abundances for different elements present a very good agreement with the chemical abundances obtained from H II regions and B stars (see Figure 3.5), due to the inside-out scenario. In Figure 3.5 it can be seen that the stellar C observed values are smaller than predicted by the model, while the N observed values are higher than the predicted ones. This differences are due to the conversion of C into N in the B-star atmospheres.

It is important to note that if our model had been built to reproduce the gaseous abundances from CELs without any type of correction, the m_{up} would have been less than 40 $M_{\odot}$. With this low m_{up} it would be difficult to explain the ionized degree observed in most of the H II regions of M33. Moreover, the corrected gaseous values are in excellent agreement with the stellar abundances, which do not need corrections, see section 3.3.5 for details.

When we considered the original Ar yields by Kobayashi et al. (2006), the CEMs predicted 0.28 dex lower than those determined in H II regions shown. The-

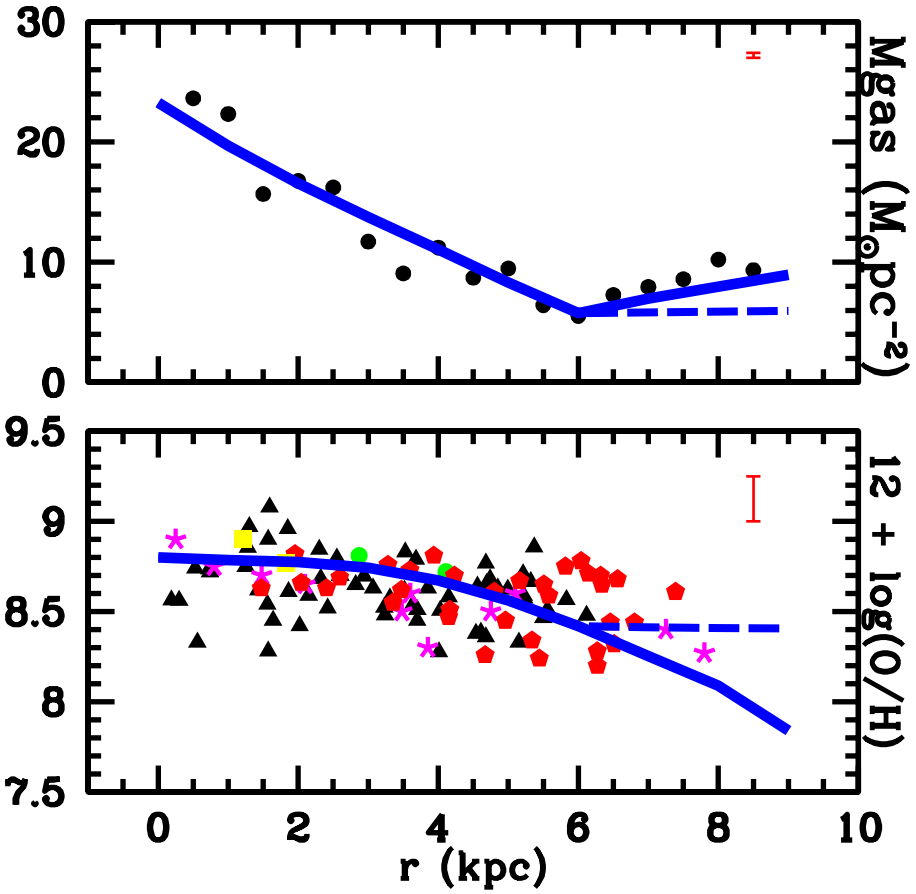

Figura 3.3: Radial distributions of the gas mass and O/H abundance at the present time, CEM1 (dashed blue line) and CEM2 (best model, solid blue line). Observational data as Figures 3.1 and 3.2. The error bars represent the average errors. Note that the gas-mass error is smaller than symbol size.

refore the Ar yields were doubled in order to reproduce the absolute value of the Ar/H gradient. The same factor was required by Hernández-Martínez et al. (2011) in the CEMs for NGC 6822, a dwarf irregular galaxy of the Local Group, for matching the Ar/H values in planetary nebulae and H II regions. The Ar yields computed by stellar evolution models could not be checked previously to our work, because the abundance of this element has not been determined from stars in the Solar Neighborhood (Timmes et al. 1995, Romano et al. 2010, Kobayashi et al. 2011).

For $r > 6$ kpc CEM1 predicts flattenings for: $M_{gas}(r)$, $SFR(r)$, $M_{stars}(r)$, and chemical gradients (see Figures 3.3, 3.4, and 3.5), that is due to the almost flat profile of the total mass adopted, and the slow rate of the gas infall. The predicted M_{gas} is in disagreement with the updated observations, which show an increase of M_{gas} with r, increase that might due to gas flows (Spitoni & Matteucci 2011) or to recent mergers (Kewley et al. 2010). That still remains an open problem, because the gas flows are more important towards the galactic center than to the outer regions, and mergers could not explain an azimuthal increase of the M_{gas} surface density. Similarly, the model does not match the SFR and M_{stars} as a function of r, since the profiles of both observations have a simple exponential decrease with r. In the case of the chemical gradients the observational data for the outer disk of M33 are insufficient to test the flattenings predicted by this model.

It is important to note that for $r > 6$ kpc the observed M_{gas}, $M_{stars}(r)$, and SFR for the present time are not consistent with a Kennicutt-Smichdt law, with constant star formation efficiency. Therefore our CEM1 cannot reproduce simultaneously those observations while we assume a ν constant in space and time.

Therefore for $r > 6$ kpc, we tried to reproduce the observations by applying in CEM1 different M_{gas} threshold values for the star formation, but the results were not consistent with the observations. Assuming thresholds higher that 5 $M_{\odot} pc^{-2}$ the $M_{gas}(r)$ was reproduced, but the chemical abundances obtained were extremely low, due to a low star formation and therefore a smaller production of metals. With thresholds lower that 5 $M_{\odot} pc^{-2}$ the values were very similar to those predicted with CEM1.

CEM with variable ν. The best model

Based on the above model, that assumes thresholds in the SFR, we realized that the CEMs need a reduction of the SFR efficiency only for recent times, but not for past times, in order to explain the current $M_{gas}(r)$, $M_{stars}(r)$, $SFR(r)$, and O/H(r) radial distributions for $r > 6$ kpc. If that reduction is considered during most of the evolution, the predicted O/H(r) in the outer regions decreases by several dexs.

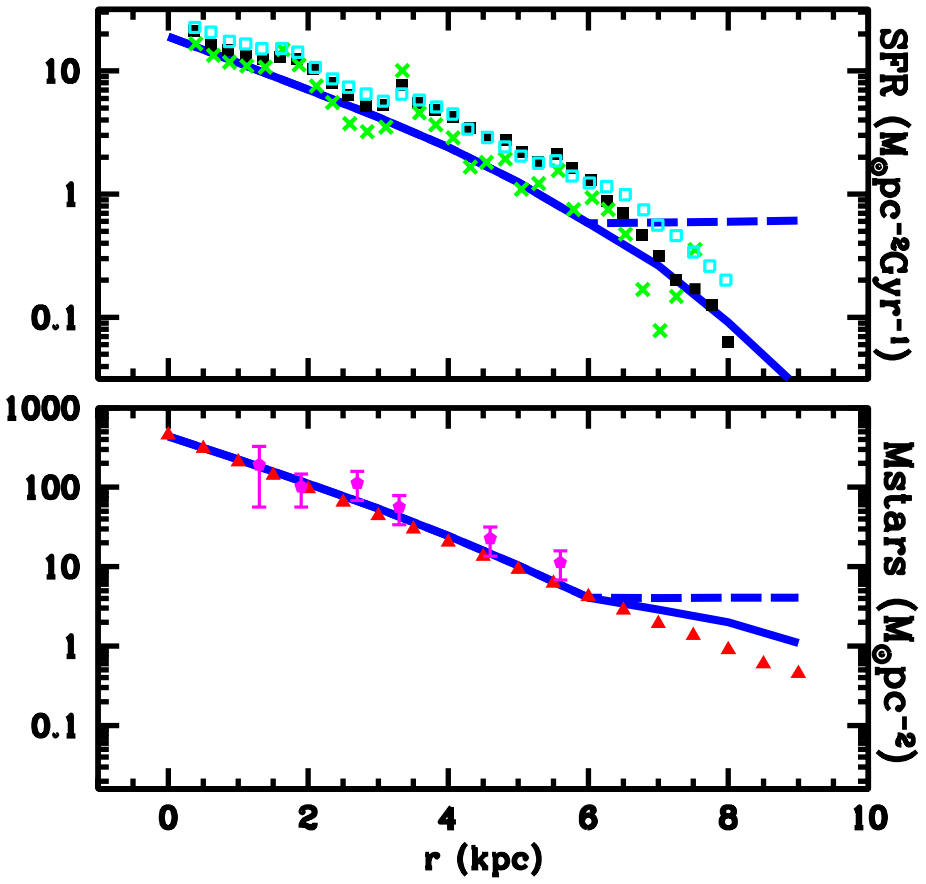

Figura 3.4: Top panel: radial distribution of the star formation rate at the present time, CEM1 (dashed blue line) and CEM2 (best model, solid blue line). Observational data by Verley et al. (2009): H_α (crosses green), FUV (filled black squares), and FIR (empty cyan squares), see section 3.3.4. Bottom panel: radial distribution of the stellar mass at the present time, CEM1 (dashed blue line) and CEM2 (best model, solid blue line). Observational data: living stellar mass by Corbelli (2003) and by Saburova & Zasov (2012), plus stellar remnants mass according to Carigi & Peimbert (2011) (filled red triangles and filled magenta pentagons, respectively).

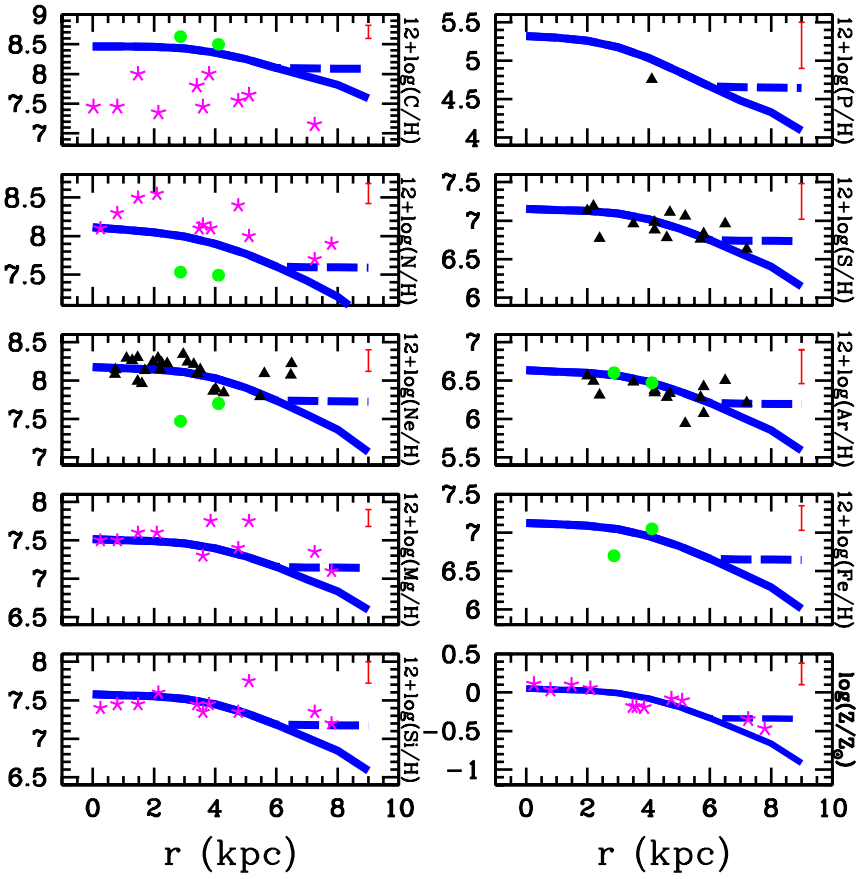

Figura 3.5: Radial distribution of C/H, N/H, Ne/H, Mg/H, Si/H, P/H, S/H, Ar/H, Fe/H, and $Z/Z_{\odot}$ abundances, CEM1 (dashed blue line) and CEM2 (best model, solid blue line). Observational data: a) Gaseous and dust values in H II regions by several authors (filled green circles and filled black triangles), b) B supergiants by Urbaneja et al. (2005) (magenta asterisks). See section 3.3.5. The error bars represent the average errors.

Therefore, we built CEM2, with the star formation efficiency, ν, variable in space and time, only for $r > 6$ kpc. We adopted $\nu = 0.007\ (M_{\odot}pc)^{-0.4}Gyr^{-1}$ for $r = 7$ kpc, and from $t = 9$ Gyr; $\nu = 0.002\ (M_{\odot}pc)^{-0.4}Gyr^{-1}$for $r = 8$ kpc, and from $t = 8$ Gyr; and $\nu = 0.0005\ (M_{\odot}pc)^{-0.4}Gyr^{-1}$ for $r = 9$ kpc, and from $t = 6$ Gyr. That indicates a reduction of SFR with the galactocentric distance, earlier at higher r, according to the warp effects in the disk (Sánchez-Blázquez et al. 2009).

In Figures 3.3 and 3.4 we show the very good agreement of $M_{gas}(r)$ and $SFR(r)$ obtained from CEM2. Moreover this model considerably improves the agreement of $M_{stars}(r)$ for $r > 7$ kpc, but the predicted values are still 2 times higher than the observations. An updated stellar profile is needed in order to refine the star formation efficiency in the outer part of the disk. In addition, CEM2 predicts chemical gradients for the 10 elements and $Z/Z_{\odot}$ that adjust very well the observations, see Figures 3.3 and 3.5. Based on the improvement in the agreements, we consider that the CEM2 is our best model.

In Figure 3.6 we present the evolution of the main results of our best model: infall, M_{gas}, SFR, and M_{stars} radial distributions at four times: 1, 5, 9, and 13 Gyr. For $r < 6$ kpc, the radial distributions behave as an inside-out model predicts (Naab & Ostriker 2006, Carigi & Peimbert 2008). The high increase in the absolute value of M_{gas}, SFR, and M_{stars} between 1 and 5 Gyr is due to the enormous amount of material that falls to form the disk during these 4 Gyrs. At this point it is worth to remind that the disk formation starts at 1 Gyr. For $r > 6$ kpc and $t = 9$ and 13 Gyr the SFR decreases with r and the M_{gas} increases with r due to the level infall rate and the diminished SFR.

In Figure 3.7 we show the evolution of the radial distributions of C/H, O/H, and Fe/H predicted by our best model at four times: 1, 5, 9, and 13 Gyr. For $r < 6$ kpc the gradients evolve as the inside-out scenario sets down (Carigi 1996). For $r > 6$ kpc and $t \leq 6$ Gyr, the gradients are space flat due to the M_{tot} behavior, the infall, and the SFR are almost space constant for those radius, while the absolute values of the gradients increase with time due to the SFR increases. Nevertheless, for $t > 6$ Gyr, the gradients get steep due to the reduction of the SFR in the outer parts, together with the gas dilution effects of the primordial infall.

In Figure 3.8 we present the evolution of the star formation rate and infall rate for six galactocentric distances: 2, 4, 6, 7, 8 and 9 kpc. For all radii, the galaxy formation follows a slow inside-out scenario. Specifically, for $r < 6$ kpc, the inner parts were built faster than the outer parts, while for $r > 6$ kpc, the outer parts were built almost simultaneously (bottom panel). Since the SFR depends on M_{gas}, M_{gas} depends on infall, and we assumed the same SFR efficiency for $r < 6$ kpc it follows that the stars formed under an inside-out scenario (top panel), as the

galaxy formed. Therefore, for $r < 6$ kpc the average stellar age decreases with r. Nevertheless, for $r > 6$ kpc we adopted SFR efficiencies that decrease earlier with r, causing a stellar formation that follows an outside-in scenario (central panel), while the galaxy formation is almost homogeneous. Consequently, for $r > 6$ kpc, the average stellar age increases with r.

From our best model, we show that the variations in the star formation efficiency for $r > 6$ kpc can match better the $M_{gas}(r)$ and $SFR(r)$ observed, the $M_{stars}(r)$ and the chemical gradients. Therefore a lower SFR and variable in space and time can explain in a more refined way the behavior for outer radii. The decrease of the SFR may be due to the reduction of molecular gas in external radii necessary to form stars, or to warp effects as mentioned previously.

3.6.2. The $\Delta Y/\Delta O$ ratio

The study of the $\Delta Y/\Delta O$ ratio is important to check the consistency of the chemical evolution models since He is produced by LIMS and MS, while O is only produced by MS. For this reason the $\Delta Y/\Delta O$ ratio depends on: i) the IMF, ii) the SFR because ΔO is in agreement with the instant recycling approximation and ΔY is not, and iii) the Y and O yields because they are metal dependent.

The only H II region in M33 that has determinations of ΔY and ΔO of high accuracy is NGC 604 (Esteban et al. 2002, 2009). For the He/H ratio we will use the results by Esteban et al. (2002) that considered the effect of the underlying absorption of the He I lines, while E09 did not. For the O/H ratio we will use the results by E09 because they did observe the 3727 [O II] line and determined with higher accuracy the O II recombination line intensities than Esteban et al.(2002). The gaseous O/H ratio amounts to 12 + log(O/H) = 8.60. The total value including the fraction of O atoms embedded in dust amounts to 8.71 dex (PP10).

To determine the production of helium in M33 we need to compare the present abundance of Y with the primordial helium abundance Y_p. The Y determination by Esteban et al.(2002) is based on the He^+ recombination coefficients by Smits (1996) while the primordial helium value of $Y_p = 0.2477$ by Peimbert et al. (2007), used in this paper, is based on the He^+ recombination coefficients by Porter et al. (2005, 2007). Therefore to determine $\Delta Y = Y - Y_p$ we recomputed the values by Esteban et al. (2002) using the results by Porter et al. and found that the Y value of 0.2641 by Esteban et al. had to be increased to 0.2682, it should be noted that as long as the Y and Y_p abundances are computed with the same He^+ recombination coefficients, ΔY is not affected by small improvements on the He^+ recombination coefficients.

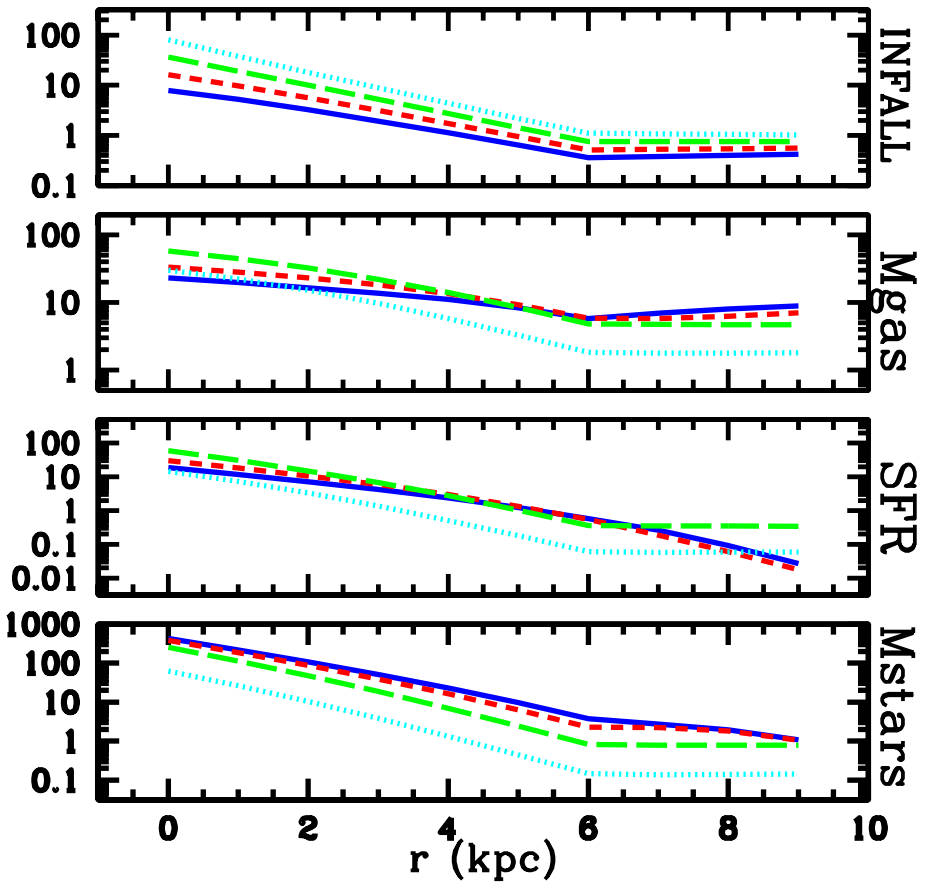

Figura 3.6: Radial distributions of: Infall ($M_\odot pc^{-2}Gyr^{-1}$), M_{gas} ($M_\odot pc^{-2}$), SFR ($M_\odot pc^{-2}Gyr^{-1}$), and M_{stars} ($M_\odot pc^{-2}$) for our best model (CEM2) at four times: 1, 5, 9, and 13 Gyr (dotted cyan, long-dashed green, short-dashed red, and solid blue lines, respectively).

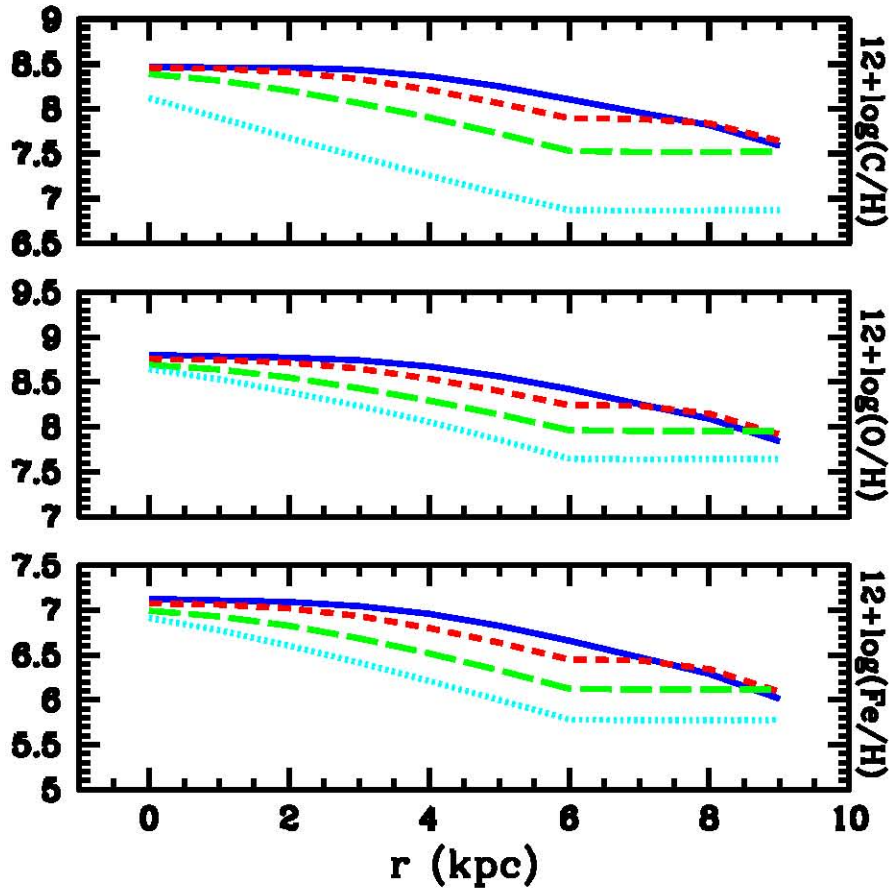

Figura 3.7: Radial distributions of C/H, O/H, and Fe/H abundances for our best model (CEM2) at four times: 1, 5, 9, and 13 Gyr, lines as Figure 3.7.

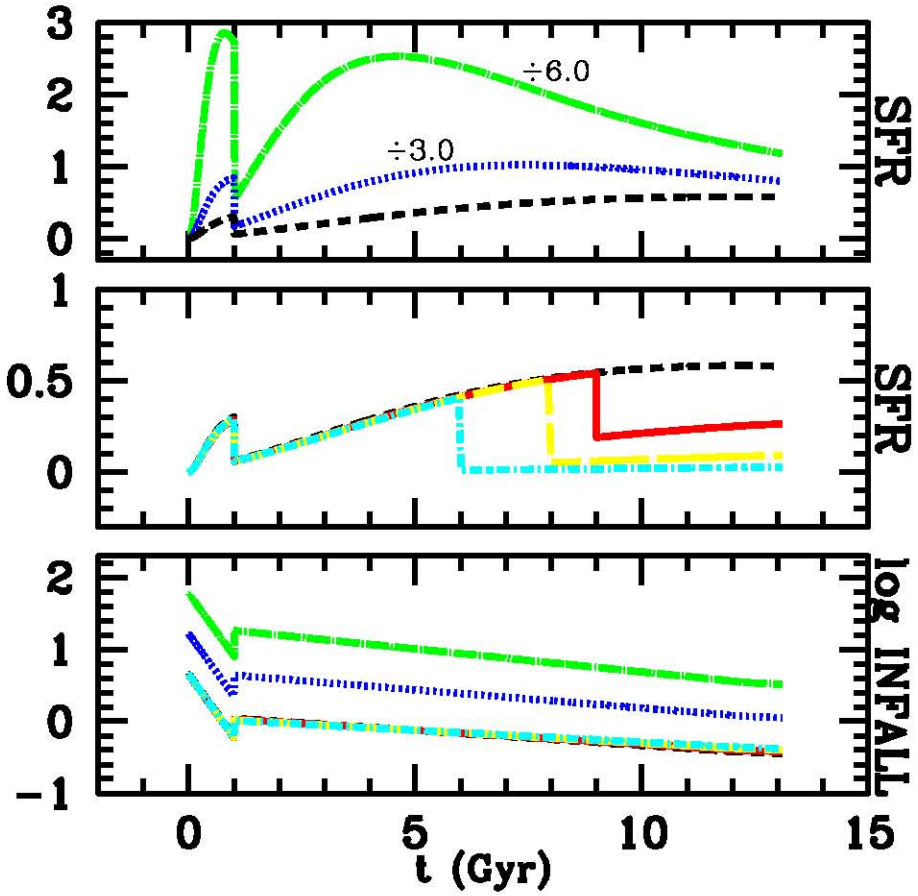

Figura 3.8: Evolution of: *SFR* ($M_{\odot}pc^{-2}Gyr^{-1}$), top and medium panels, and of: Infall ($M_{\odot}pc^{-2}Gyr^{-1}$),bottom panel, for our best model (CEM2) at six radii: 2, 4, 6, 7, 8 and 9 kpc (dot-long-dashed green, dotted blue, short-dashed black, solid red, long-dashed yellow, and dot-short-dashed cyan lines, respectively). In the top panel the *SFR* for r = 2 and 4 kpc have been divided by 6 and 3 respectively.

Cuadro 3.1: Abundances of Helium, Oxygen, and Heavy Elements by Mass.

Parameter	$t^2 \neq 0.000$	*CEM*2
Y	$0.2682^a \pm 0.0040$	0.2651
ΔY	$0.0205^b \pm 0.0048$	0.0174
O	$0.00590^c \pm 0.00090$	0.00532
$\Delta Y/\Delta O$	3.47 ± 0.79	3.29
Z	$0.0139^d \pm 0.0021$	0.0116
$\Delta Y/\Delta Z$	1.47 ± 0.34	1.51

a Taken from Esteban et al. (2002).
b Considering $Y_p = 0.2477$ by Peimbert et al. (2007).
c Taken from Esteban et al. (2009).
d Considering $O = 0.43Z$.

In Table 1 we present the observed $\Delta Y/\Delta O$ for NGC 604 and compare it with that predicted by our chemical evolution model. We have considered a galactocentric distance of 4.11 kpc for NGC 604. We also present the $\Delta Y/\Delta Z$ ratio where we have assumed that the O abundance represents 43.3 % of the total heavy element abundance Z, as is the case in the protosolar abundances (Asplund et al. 2009).

In Figure 3.9 we present the evolution of ΔY versus ΔO and of the $\Delta Y/\Delta O$ ratio predicted by our model for r =4.11 kpc and compare both results with the observed values. Since CEM1 and CEM2 are identical for $r \leq 6$ kpc, we present only the CEM2 results. The good agreement between the model and the observational restrictions imply that the ingredients used in the model, mainly the IMF and the yields are adequate for this galaxy. For other galactocentric radii ΔY vs ΔO the evolution of M33 is similar to ΔY vs ΔO evolution of the Milky Way, see Figure 7 by Carigi & Peimbert (2011).

3.7. Inside-out and outside-in stellar formation in the Local Group of galaxies

The Local Group is formed by two massive spiral galaxies (M31 and the MW), about 70 minor galaxies (Irr, cE, dIrrs, dSphs, dIrr/dSphs) and one small spiral galaxy (M33) (McConnachie 2012).

The spiral galaxies of the Local Group present negative B-V and chemical gradients, indicating a negative age gradient, being the inner parts dominated by old populations and the outer parts by young populations. That suggests an inside-out stellar and galactic formation (Carigi & Peimbert 2011, Carigi, Meneses-Goytia

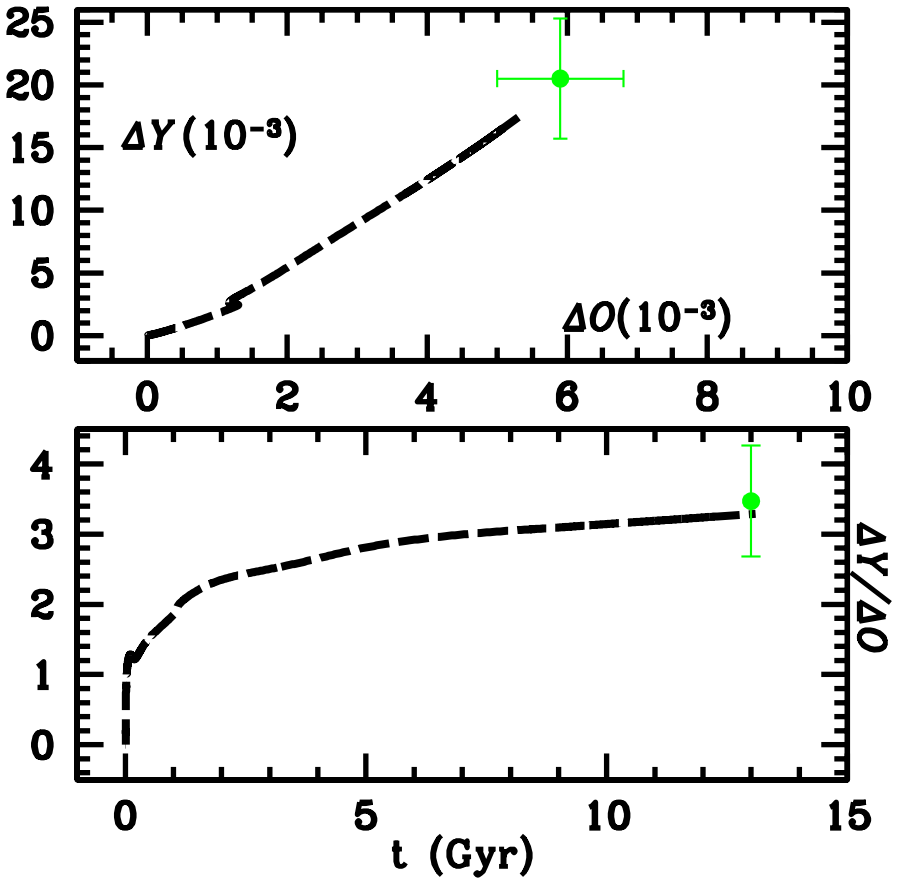

Figura 3.9: Chemical evolution models at r = 4.11 kpc (long-dashed black). Top panel: ΔY vs ΔO evolution. Bottom panel: $\Delta Y/\Delta O$ evolution. Observational data: NGC 604 at r = 4.11 kpc by Esteban et al. (2002, 2009) (green filled circles). The shown values include the corrections by the t^2 factor (for *He* and *O*) and by dust depletion (only for *O*). See section 3.6.2 for details.

& García-Rojas 2012).

Many dwarf galaxies of the Local Group present positive B-V gradient and consequently positive age gradient, being the inner parts dominated by young populations and the outer parts by old populations. That suggests an outside-in stellar and galactic formation (de Boer et at. 2012a,b; Hidalgo 2012; Hidalgo et al. 2012 and references therein).

In our work, we found that the inner parts of M33 ($r < 6$ kpc) behave like M31 or MW (the mean stellar age decreases with radius), while the outer parts of M33 ($r > 6$ kpc) behave as dwarf galaxies (the mean stellar age increases with radius). Therefore M33, a galaxy with an intermediate mass, presents characteristics similar to the smallest and the biggest galaxies, in the respective mass regimes, being a unique example in the Local Group that connects the formation and evolution of both types of galaxies.

In the outermost disk of some spiral galaxies outside the Local Group, flattening in the chemical gradients has been observed (Vlajic 2010; Bresolin, Kennicutt & Ryan-Weber 2012). The determination of the flatten gradient at high r is still an open question for the MW and M31 (Esteban et al. 2012 and references therein), due mainly to the inconsistency among stellar and gaseous data, and it is not found yet for M33, due to the lack of data (see section 3.3.5).

Different processes offer possible explanations for the chemical gradient flattening: a) radial stellar migrations (Roediger et al. 2012, Minchev et al. 2012) that provide the outer disk with stars born in the inner part of the galaxy and therefore enrich these external zones, b) effects of the warp that can produce decreases in the star formation (Sánchez-Blázquez et al. 2009), c) physical conditions in the distribution of gas not adequate for the star formation (deficient amount of molecular gas, gas temperature, among others), d) mixing and turbulence processes, (e) galactic scale outflows, and (f) enriched accretion (Bresolin et al).

It is important to mention that a nearly flat chemical gradient has been estimated in dwarf galaxies, based on stellar Fe/H and gaseous O/H observed values and on theoretical Z values inferred by synthetic Color-Magnitude Diagram analysis (Tolstoy, Hill & Tosi 2009).

It is worthy to remark that the direct association of the accreted baryonic mass, or galactic formation, with the SFR intensity, or stellar formation, (and vice versa) does not follow in the outer parts of M33. Consequently, the simple inference of how a galaxy forms from the star formation history could be risky, because the SFR depends on other factors, in addition to the gas amount.

3.8. Conclusions

Based on an exhaustive review of the recent observational data of M33 we computed a successfully chemical evolution model for this galaxy. From this model we reach the following conclusions.

1) The total baryonic mass surface density shows a decreasing exponential behavior as a function of r up to r = 6 kpc, beyond this radius it shows a light rise, due to the increase of the gaseous mass surface density for $r > 6$ kpc.

2) O/H abundance ratios from O-B stars agree with abundances derived from H II regions only if the RLs gaseous abundances are corrected by dust depletion. Moreover the O/H abundance ratios from O-B stars agree with CEls O/H gaseous abundances only if they are increased by the effect of temperature variations and by the fraction of O atoms embedded in dust grains.

3) From the stellar and corrected gaseous abundances, the oxygen gradient of the disk is: 12 + log(O/H) = -(0.038 ±0.008)r + (8.747 ± 0.035).

4) To reproduce the absolute value of the observed O/H gradient, we obtain that the IMF upper mass for M33 amounts to 50 $M_{\odot}$.

5) To reproduce the absolute value of the Ar/H gradient, the Ar yields need to be two times higher than the ones computed by Kobayashi et al. (2006).

6) To match the absolute value of the Fe/H gradient, the fraction of binary systems that become SNe Ia has to be 5 %. To reproduce the $< [Fe/H] >$ shown by the halo stars, the efficiency of star formation in the halo has to be 5 times larger than that adopted for the disk.

7) The $\Delta Y/\Delta O$ value equal to 3.29, predicted by the model for r = 4.11 kpc, is in very good agreement with the observed value: 3.47 ±0.79 for NGC 604, an H II region of M33.

8) No star formation thresholds based on the surface density of gas mass could explain the galactic properties for $r > 6$ kpc. It is necessary to determine thresholds as a function of the volumetric density of gas mass for the purpose of understanding the dependence on time and galactocentric radius found for the outskirts of the disk.

9) For $r > 6$ kpc, updated determinations of: stellar mass, star formation, and chemical abundances are required to try to explain the formation and evolution of the M33 outer part.

10) The inner part ($r < 6$ kpc) of M33 was formed according to a slow inside-out scenario, but the outer part ($r > 6$ kpc) was formed almost independently of the galactocentric distance.

11) For the inner part, the star formation efficiency is constant in time and

space, but for the outer part the efficiency decreases with time and galactocentric distances. The reduction of the SFR efficiency, earlier at higher r, produces an outside-in stellar formation and consequently an increase with r of the average stellar age. That radial-temporal behavior of the SFR efficiency for $r > 6$ kpc may be caused by the warp in the disk. Warps can reduce the gas volumetric density, even when the gas surface density is kept constant or increases.

Bibliografía

Asplund M., Grevesse N., Jacques A., Scott P., 2009, Annu. Rev. Astro. Astrophys., 47, 481

Barker M., Sarajedini A., 2008, MNRAS, 390, 863

Boissier S., Gil de Paz A., Boselli A., et al., 2007, ApJS, 173, 524

Bresolin F., 2011, ApJ, 730, 129

Bresolin F., Kennicutt R., Ryan-Weber E., 2012, ApJ, 750, 122

Brooks R., Wilson D., Harris W., 2004, AJ, 128, 237

Carigi L., 1996, RMxAA, 32, 179

Carigi L., Peimbert M., 2008, RMxAA, 44, 341

Carigi L., Peimbert M., 2011, RMxAA, 47, 139

Carigi L., Meneses-Goytia S., Garía-Rojas J., 2012, RMxAA, submitted (arXiv:1208.4198)

Chabrier G., 2003, ApJ, 586, L133

Chiappini C., Matteucci F., Gratton R., 1997, ApJ, 477, 765

Chiappini C., Matteucci F., Romano D., 2001, ApJ, 554, 1044

Corbelli E., Schneider E., 1997, ApJ, 479, 244

Corbelli E., 2003, MNRAS, 342, 199

Crockett N. R., Garnett D. R., Massey P., Jacoby G., 2006, ApJ, 637, 741

de Boer T., Tolstoy E., Hill V., Saha A., Olsen K., Starkenburg E., Lemasle B., Irwin M.,Battaglia G., 2012a, A&A, 539A, 103D

de Boer T., Tolstoy E., Hill V., Saha A., Olszewski E., Mateo M., Starkenburg E., Battaglia G., Walker M., 2012b, A&A, 544A, 73D

Esteban C., Peimbert M., Torres-Peimbert S., Rodríguez M., 2002, ApJ, 581, 241

Esteban C., Bresolin F., Peimbert M., García-Rojas J., Peimbert A., Mesa-Delgado A., 2009, ApJ, 700, 654 (E09)

Esteban C., Carigi L., Copetti M. V. F., García-Rojas J., Mesa-Delgado A., Castañeda H. O., 2012, MNRAS, in preparation

Ferrini F., Penco U., Palla F., 1990, A&A, 231, 391

Ferrini F., Matteucci F., Pardi C., Penco U., 1992, ApJ, 387, 138

Freedman W., Wilson C., Madore B., 1991, ApJ, 372, 455

Gil de Paz A., Boissier S., Madore B., et al., 2007, ApJS, 173, 185G

Gratier P., Braine J., Rodríguez-Fernandez N., Schuster K., et al., 2010, A&A, 522A, 3G

Greggio L., Renzini A., 1983, A&A, 118, 217

Hernández-Martínez L., Carigi L., Peña M., Peimbert M., 2011, A&A, 535, 118

Hidalgo S. L., 2011, EAS Publications Series, 48, 37

Hidalgo S. L., 2012, EPJW of Conferences, 19, 03004H

Hidalgo S. L., Monelli M., Aparicio A., Gallart C., 2012, ApJ, submitted

Hirshi R., Meynet G., Maeder A., 2005, A&A, 433, 1013

Hirshi R., 2007, A&A, 461, 571

Kang X., Chang R., Yin J., Hou J., Zhang F., Zhang Y., Han Z., 2012, MNRAS, 426, 1455

Karakas A., 2010, MNRAS, 403, 1413

Kennicutt A., 1998, ApJ, 498, 541

Kewley L., Rupke D., Jabran Z., Geller M., Barton E., 2010, ApJ, 721, L48

Kobayashi C., Umeda H., Nomoto K., Tominaga N., Ohkubo T., 2006, ApJ, 653, 1145

Kobayashi C., Karakas A., Umeda H., 2011, MNRAS, 414, 3231

Kroupa P., 2001, MNRAS, 322, 231

Kroupa P., Tout C., Gilmore G., 1993, MNRAS, 262, 545

Kwitter K. B., Aller L. H., 1981, MNRAS, 195, 939

Lebouteiller V., Kunth J., Lequeux J., Aloisi A., Désert J., Hébrard G., Lecavelier des Étangs A., Vidal-Madjar A., 2006, A&A, 459, 161

Maeder A., 1992, A&A, 264, 105

Magrini L., Vílchez J., Mampaso A., Corradi R., Leisy P., 2007a, A&A, 470, 865

Magrini L., Corbelli E., Galli D., 2007b, A&A, 470, 843

Magrini L., Stanghellini L., Corbelli E., Galli D., Villaver E., 2010, A&A, 512, A63

Marcon-Uchida M., Matteucci F., Costa R., 2010, A&A, 520, A35

Matteucci F., 2001, Astrophysics and Space Science Library, Vol. 253, The Chemical Evolution of the Galaxy (Dordrecht:Kluwer),293

McChonnachie A., 2012, AJ, 144, 4

Mesa-Delgado A., Esteban C., García-Rojas J., Luridiana V., Bautista M., Rodríguez M., López-Martín L., Peimbert M., 2009, MNRAS, 395, 855

Meynet G., Maeder A., 2002, A&A, 390, 561

Minchev I., Famaey B., Quillen A. C., Di Matteo P., Combes F., Vlajić M., Erwin P., Bland-Hawthorn J., 2012, A&A, accepted (arXiv:1203.2621)

Mollá M., Ferrini F., Díaz A., 1996, ApJ, 466, 668

Mollá M., Ferrini F., Díaz A., 1997, ApJ, 475, 519

Mollá M., & Díaz A., 2005, MNRAS, 358, 521

Monelli M., Carrera R., Gallart C., Meschin I., Aparicio A., Hidalgo S. L., Bono G., Stetson P. B., Walker A. R., 2011, EAS Publications Series, 48, 43

Naab T., Ostriker J., 2006, MNRAS, 366, 899

Nomoto K., Iwamoto N., Nakasato N., Thielemann F., Brachwitz F., Tsujimoto T., Kubo Y., Kishimotp N.,1997, NuPha, 621, 467

Pagel B., 2009, Nucleosynthesis and Chemical Evolution of Galaxies (Cambridge: Cambridge Univ. Press)

Peimbert M., Luridiana V., Peimbert A., 2007, ApJ, 666, 636

Peimbert A., Peimbert M., 2010, ApJ, 724, 791 (PP10)

Porter R. L., Bauman R. P., Ferland G. J., MacAdam K. B., 2005, ApJ, 622, L73

Porter R. L., Ferland G. J., MacAdam K. B., 2007, ApJ, 657, 327

Prantzos N., 2008, EAS Publications Series, 32, 311 (arXiv:0709.0833)

Przybilla N., Firnstein M., Nieva M. F., Menet G., Maeder A., 2010, A&A, 517, A38

Regan M., Vogel S., 1994, ApJ, 675, 1213

Roediger J., Courteau S., Sánchez-Blázquez P., McDonald M., 2012, ApJ, 758, 41R

Romano D., Chiappini C., Matteucci F., Tosi M., 2005, A&A, 430, 491

Romano D., Karakas A., Tosi M., Matteucci F., 2010, A&A, 522, 32

Rosolowsky E., Simon J., 2008, ApJ, 434, 536

Saburova A., Zasov A., 2012, Astronomy Letters, 38, 139

Sánchez-Blázquez P., Courty S., Gibson B., Brook C., 2009, MNRAS, 398, 591S

Sarajedini A., Geisler D., Schommer R., 2000, AJ, 120, 2434

Smits D. P., 1996, MNRAS, 278, 683

Spitoni E., Matteucci F., 2011, A&A, 531, 72

Timmes F., Woosley S., Weaver T., 1995, ApJSS, 98, 617

Tinsley B., 1980, Fundam. Cosmic Phys., 5, 287

Tolstoy E., Vanessa H., Tosi M., 2009, Annu. Rev. Astro. Astrophys., 47, 371

Urbaneja M., Herrero A., Kudritzki R., Najarro F., Smartt S., Puls J., Lennon D., Corral L., 2005, ApJ, 635, 311

Verley S., Corbelli E., Giovanardi C., Hunt L., 2009, A&A, 493, 453

Vílchez J. M., Pagel B. J., Díaz A. I., Terlevich E., Edmunds M. G., 1988, MNRAS, 235, 633

Vlajić M., 2010, PASA, 27, 252

Willner S., Nelson-Patel K., 2002, ApJ, 568, 679

Capítulo 4

Star formation efficiency and flattened gradients in M31

4.1. Abstract

We present and discuss results from a chemical evolution model for M31 based on a pronounced inside-out scenario for the galactic formation. The model has been built to reproduce three observational constraints of the M31 disk: the radial distributions of the total baryonic mass, the gas mass, and the O/H abundance. The model shows excellent agreement, throughout the galactic disk, with the observed radial distributions of the SFR, the stellar mass, and with gradients for fifteen chemical elements. The observed gas mass profile of M31 presents a peak between 9 and 11 kpc and the observed SFR diminishes for $r > 12$ kpc. To obtain a consistent set of O/H values from H II regions, we correct those gaseous abundances due to the effect of temperature variations and O trapped in dust grains. From reproducing the radial distributions of the gas mass, we find that the star formation efficiency is variable in space, for the whole disk, and is constant in time for most of the evolution ($t < 12.8$ Gyr). From reproducing the radial distributions of the SFR, we find that the efficiency decreases almost to zero for $12.8 < t$ (Gyr) < 13.0 and $r > 12$ kpc. The predicted radial distribution of each Xi/H ratio shows three different gradients, all of them flatten at different rates due to the r-dependence of the the star formation efficiency and the inside-out galactic formation.

4.2. Introduction

Chemical evolution models (CEMs) are useful to predict the chemical history of galaxies. Therefore, CEMs are able to infer, in general, how galaxies and stars have been formed and how efficient are the stars to produce chemical elements.

In this paper we present a successful CEM for the Andromeda galaxy, M31, the largest spiral galaxy in the Local Group. M31 is an Sb galaxy located at a distance of 744±33 kpc (Villardell et al. 2010) and has a deprojected semi-major axis of 70±10 kpc. The baryonic mass of M31 is about 1.2 times larger than that of the Milky Way (Widrow, Perrett & Suyu 2003).

There are some chemical evolution models of M31 in the literature, that were built trying to reproduce the observed radial distributions of: i) the gas mass (M_{gas}) without considering the He and Z contribution and ii) the O/H gaseous values of the H II regions, without consider the correction in the O/H ratio due to temperature variations and without considering the correction due to the fraction of O trapped in dust grains, these two corrections taken together reduce the true O/H value in the H II regions by about 0.3 dex (e. g. Peimbert et al. 2007, Peimbert & Peimbert 2010, Peña -Guerrero et al. 2012). The temperature variations can be represented by the mean square temperature variation t^2 (Peimbert 1967). Below we describe briefly the most recent CEMs of M31, for more details of these CEMs see the paper of the respective authors.

Renda et al. (2005) presented a set of CEMs for M31, based on the SFR formulation by Wyse & Silk (1989), with a star formation efficiency constant in time and space, where the SFR is inversely proportional to the radius. They used the initial mass function (IMF) by Kroupa, Tout & Gilmore (1993). Their best model reproduced reasonably well the observations available when they developed that work.

Mattsson (2008) built two CEMs of M31, assuming a star formation law that combines a Silk law and a Schmidt law (Boissier et al. 2003), with a star formation efficiency constant in time and space, and dependent of the angular frequency of the galactic disk. He used an IMF similar to Scalo's one (1986), but considered a larger fraction of very low mass stars and substellar objects. This model could not reproduce the observational radial profile of the gas mass and adjusted moderately well the observed of O/H abundances considered by him.

Yin et al. (2009) constructed a CEM for M31, considering a modified star formation Kennicutt-Schmidth law (Fu et al. 2009), with a star formation efficiency constant in time and space, and the SFR is inversely proportional to the radius. They assumed the IMF by Kroupa, Tout & Gilmore (1993). Their model did not

adjust the distribution of the gas mass for $r < 8$ kpc. They obtained a good fit with the observed values of O/H.

Marcon-Uchida, Matteucci & Costa (2010) developed a set of CEMs of M31. They used a SFR that follows the Kennicutt-Schmidt law (Kennicutt 1998), with a star formation efficiency variable with radius, and adopting a gas mass threshold for star formation of 5 $M_\odot$ pc^{-2}. They assumed the IMF by Kroupa, Tout & Gilmore (1993). Their best model failed to reproduce the distribution of gas mass and presents a reasonable fit of the O/H abundances.

Carigi, García-Rojas & Meneses-Goytia (2013) built a CEM under the instantaneous recycling approximation, adopting a SFR following the Kennicutt-Schmidt law (Kennicutt 1998) with a star formation efficiency constant in time and in radius. They adopted the IMF by Kroupa, Tout & Gilmore (1993). Their CEM does not reproduce the distribution observed of the gas mass and reproduces well the most probable O/H gradient based in the observational data.

Spitoni, Matteucci & Marcon-Uchida (2013) presented a study of the effects of galactic fountains and radial gas flows on the chemical evolution models. Their study is based on the CEM by Marcon-Uchida, Matteucci & Costa (2010), described above. They concluded that galactic fountains are not an important factor in the chemical evolution of the galactic disk. Moreover they found that the radial gas flows produce the same effect on the O/H gradient that adopting a threshold and an r-dependent efficiency of the SFR.

Since the previous models cannot explain the radial distribution of the gas mass of the M31 disk, and currently there are more precise observations, we have decided to built a new CEM for M31. Our CEM reproduces successfully and for the entire disk, the updated an more precise values of the radial distributions of the total baryonic mass, the gas mass and the O/H abundances, and also shows good agreement with the radial distributions of the star formation rate, the stellar mass, and the gradients of other fifteen chemical elements.

Throughout this paper, we adopt the usual notation X, Y, and Z to represent the hydrogen, helium and heavy element abundances by mass, while the abundances by number are represented without italics. In Section 4.3, we describe the observational constraints used in this paper. In Section 4.4, we present the features of our CEM. In Section 4.5, we present the main results of our CEM. In Section 4.6, we discuss the helium and oxygen enrichment. The conclusions are presented in Section 4.7.

4.3. Observational constraints

The CEM of M31 is built to reproduce three main observational constraints of the galactic disk at the present time: the radial distributions of the total baryonic mass, the gas mass, and the O/H ratio. Also the predictions of the CEM are compared with other observational constraints of the M31 disk, the radial distributions of: the star formation rate, the stellar mass, the abundances of fifteen chemical elements relative to H and the total metallicity, Z.

4.3.1. Radial distribution of the mass surface densities

Gas mass, $M_{gas}(r)$

The radial profile of the gas mass, $M_{gas}(r)$ ($M_{\odot}pc^{-2}$), represents the atomic and molecular gas that contains all the chemical elements, *i.e.* $M_{gas}(r) = M_X(\mathrm{r}) + M_Y(\mathrm{r}) + M_Z(r)$. We obtain $M_X(r)$, by adding the atomic and molecular components, that was provided by Tabatabaei (2013, private communication), based on Nieten et al. (2006), and we correct by thw inclination angle of 75° (Berkhuijsen 1977, Braun 1991).

We computed $M_Y(r)$ and $M_Z(r)$ from the following relations:

i) The proportion between gas mass of a given element, M_i, and the chemical abundance by mass of this element, X_i, is $M_i = X_i \times M_{gas}$. Specifically: $M_Y(r)/M_X(r) = Y(r)/X(r)$ and $M_Z(r)/M_X(r) = Z(r)/X(r)$.

ii) The normalization of the chemical abundances by mass: $X(r) = 1 - Y(r) - Z(r)$.

iii) The $Y(r)$ and $O(r)$ enrichment by Carigi & Peimbert (2008): $Y(r) = 0.2477 + 3.3O(r)$.

iv) The transformation of O/X (by mass) to O/H (by number): $O(r)/X(r) = 16\,(\mathrm{O/H})(r)$.

v) The O/H gradient determined in this paper (see eq. 4.4).

vi) The conservation of the solar Z / (O/H) ratio in the interstellar medium: $Z(r)/(O/H)(r) = Z_{\odot}/(O/H)_{\odot}$.

vii) The protosolar values of $Z_{\odot} = 0.0142$ and $12 + \log(\mathrm{O/H})_{\odot} = 8.73$ dex by Asplund et al. (2009).

The contributions of M_Y and M_Z increase the gas mass surface density approximately by a factor of 1.2, relative to M_X. It is worthy to note that the radial distribution of the corrected gas mass shows a broad peak between 9 and 11 kpc (see Figure 4.1, top panel) that is not present in the MW (see Esteban et al. 2013).

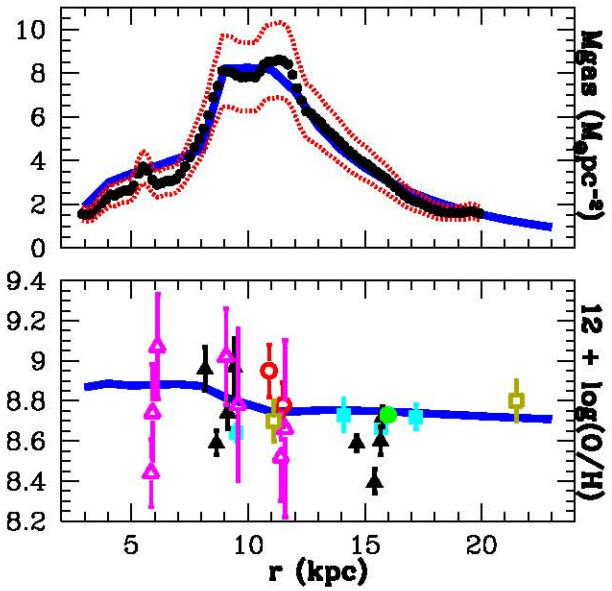

Figura 4.1: Top panel: radial distribution of the gas mass at the present time of our chemical evolution model (CEM, solid blue line). Observational data by Nieten et al. (2006) including the contributions of helium and metals (black circles, see Section 2.1.1). The red dotted lines represent the values within one σ error. Bottom panel: radial distribution of the O/H ratios at the present time, CEM (solid blue line). Observational data: (i) gaseous values from H II regions corrected by us for temperature variations (t^2 factor) and dust depletion (see Section 4.3.3), Zurita & Bresolin (2012) (filled black triangles), Sanders et al. (2012) (filled cyan squares), and Esteban et al. (2009) (filled green circle); (ii) stellar values, Przybilla et al. (2006) (empty red circles), Trundle et al. (2002) (empty magenta triangles), and Venn et al. (2000) (empty gold squares). The vertical lines represent one σ error.

Stellar mass, $M_{stars}(r)$

We use the luminosity profile of the M31 disk to obtain the radial distribution of the mass surface density of living stars, $M_{starL}(r)(\mathrm{M_\odot pc^{-2}})$. We consider an average of the disk scale lengths from three bands: *R*, *K,* and *I* by Walterbos & Kennicutt (1988), Hiromoto et al. (1983), and Worthey et al. (2005), respectively, and we obtain a disk scale length equal to r_{disk}=5.5 kpc. We calculate the central density by the integration of the $M_{starL}(r)$ over the surface of the galactic disk in order to reproduce the stellar mass estimated for the M31 disk, which is $6{\times}10^{10}\mathrm{M_\odot}$ (Tamm et al. 2012).

In addition, we take into account the contribution to the stellar mass due to the stellar remnants, $M_{starR}(r)(\mathrm{M_\odot pc^{-2}})$, with a value equal to 13 percent of the living stellar mass, according to the computation for the Galaxy (private communication with L. Carigi and M. Peimbert 2011). Therefore, the radial distribution of the total stellar profile is given by:

$$M_{stars}(r) = M_{starL}(r) + M_{starR}(r) = 230e^{(-r/5.5kpc)}, \tag{4.1}$$

see Figure 4.2, top panel.

Baryonic mass, $M_{tot}(r)$

The total baryonic mass is the sum of the profiles of the gas mass and the total stellar mass, *i.e.* $M_{tot}(r) = M_{gas}(r) + M_{stars}(r)$. The radial distribution of the total baryonic mass shows a single exponential profile, given by:

$$M_{tot}(r) = 240e^{(-r/5.7kpc)}. \tag{4.2}$$

4.3.2. Radial distribution of the star formation rate, $SFR(r)$

M31 is a galaxy with a relatively quiescent star formation at the present time, considering that the values estimated of its total star formation rate are $\sim 0.4{-}1.0$ $\mathrm{M_\odot\ yr^{-1}}$ (Williams 2003a,b; Barmby et al. 2006), a 1/4−1/2 of the values estimated for the Milky Way, $\sim 1.5{-}2.3$ $\mathrm{M_\odot\ yr^{-1}}$ (Kennicutt & Evans 2012).

To compare with our CEM, we use the radial distribution of the star formation rate obtained by Boissier et al. (2007), estimated from UV profiles, corrected for extinction by dust (see Figure 4.2, bottom panel). The observations show that the $SFR(r)$ and $M_{gas}(r)$ do not obey a Kennicutt-Schmidt law with a constant ν, due to a decrease in the observed values of the *SFR*.

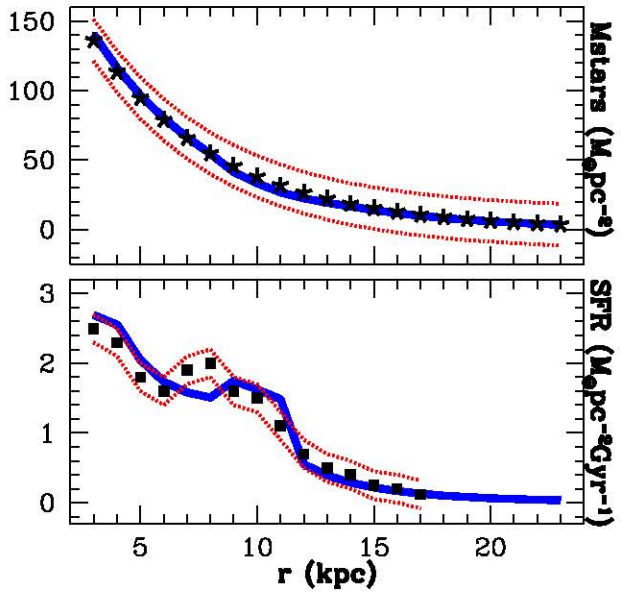

Figura 4.2: Top panel: radial distribution of the total stellar mass at the present time, CEM (solid blue line). Observational data: an average of the disk scale length equal to 5.5 kpc, and a central density equal to 230 $M_{\odot}$ pc^{-2} (black stars, see Section 4.3.1). Bottom panel: radial distribution of the *SFR* at the present time, CEM (solid blue line). Observational data: Boissier et al. (2007) (filled black squares, see Section 4.3.1). The red dotted lines represent the values within one σ error.

4.3.3. Radial distribution of the chemical abundance ratios, $X_i(r)/H(r)$

As observational constraints at the present time, we consider the most recent studies on the chemical abundances of H II regions and of supergiant stars, because both represent the current chemistry of the gas in the M31 disk.

The gaseous O/H ratios determined for the H II regions along the M31 disk do not show a clear gradient, due to, possibly, different empirical calibration methods used in the derivation of the electronic temperatures of the gas. We take into account the recalibration method called Corrected Auroral Line Method (CALM), presented by Peña-Guerrero, Peimbert & Peimbert (2012). In this calibration method, they considered the temperature inhomogeneity in H II regions given by the t^2 factor (Peimbert 1967; Peimbert et al. 2007a), and the fraction of oxygen atoms trapped into dust grains (Peimbert & Peimbert 2010). We use their equation to obtain the corrected oxygen abundance given by:

$$(12 + log(O/H)_{CALM}) = 1.0825\ (12 + log(O/H)_{4363/5007}) - 0.375, \qquad (4.3)$$

where $(O/H)_{4363/5007}$ correspond to the abundance estimated with the temperature derived from the [O III] (4363/5007). Consequently, we use only the chemical abundances estimated from the brightest H II regions, where the auroral lines can be observed. Recently Croxall et al. (2013) have determined O/H ratios for the galaxy NGC 628 based on the infrared lines of [O III]. These lines do not depend on the temperature structure of the H II region and the abundances are in good agreement with the CALM calibration by Peña-Guerrero et al. (2012).

Zurita & Bresolin (2012) derived the N/H, O/H, S/H, Ar/H, and Ne/H abundances for eight H II regions using collisional excitation lines (CELs), and assuming the [O III] (4363/5007) temperature. Since CELs are sensitive to spatial temperature variations in the H II regions, and considering the dust-phase component of the oxygen, their O/H ratios are corrected using equation (4.3). In the case of the N/H, S/H, Ar/H, and Ne/H abundances we correct by the t^2 factor, increasing the gaseous values by 0.19, 0.21, 0.24, and 0.26 dex, respectively (Esteban et al. 2009, E09). The correction due to the fraction of N and S embedded in dust has not been estimated for H II regions and is not taken into account; while for Ar and Ne, the correction is zero, because they are noble gases and are not expected to be embedded in dust grains.

Sanders et al. (2012) determined the N/H and O/H ratios for hundreds of H II regions from CELs, but only for four H II regions they used the [O III] (4363/5007) temperature. We correct the O/H gaseous values for these four regions using equation 4.3. The N/H values are increased by 0.26 dex, due to the t^2 factor (E09), and

no correction is made for the fraction of N atoms embedded in dust grains.

Esteban et al. 2009 obtained the C/H, N/H, O/H, Ne/H, S/H, Ar/H, and Fe/H abundances in one H II region: K932, using recombination lines (RLs) and the [O III] (4363/5007) temperature. The RL ratios are not sensitive to temperature variations, therefore, the abundances based on RL ratios are not corrected by the t^2 factor. We correct the C/H, O/H and Fe/H abundances by dust depletion, increasing the gaseous values by 0.10, 0.11 and 1.00 dex, respectively (E09; Mesa-Delgado et al. 2009; Peimbert & Peimbert 2010). The N/H, Ne/H, and Ar/H abundances by E09 are not increased by dust depletion.

Considering the corrected O/H values from H II regions and their estimated error, we obtain the oxygen gradient in the 7-18 kpc region of the M31 disk:

$$12 + log(O/H) = (8.73 \pm 0.06) - (r - 12)(0.013 \pm 0.006). \quad (4.4)$$

This fit is obtained mainly based on the H II data located between 7 and 18 kpc. This is because for higher r values, we have only one object, and for smaller r values, the observations present very large error bars.

We compute the Z value of each H II region, adding all chemical abundances and dividing by the sum of the protosolar abundances (Asplund et al. 2009) of the same elements considered for each H II region, thus:

$$Z_{HII} = \frac{\Sigma(X_i)_{HII}}{\Sigma(X_i)_{\odot}} Z_{\odot}, \quad (4.5)$$

(see Figure 4.7, bottom panel).

There are several chemical abundance determinations for O, B, A and F supergiant stars in M31 that are used by us as a consistency check for the predicted O/H gradient of our CEM. Przybilla et al. (2006) derived the C/H, N/H, O/H, Mg/H, Al/H, Si/H, S/H, Sc/H, Ti/H, Cr/H, Mn/H, and Fe/H ratios for two A stars. Trundle et al. (2002) obtained the C/H, N/H, O/H, Mg/H, Al/H, Si/H, S/H, and Fe/H ratios for seven B stars. Venn et al. (2000) determined the C/H, O/H, Mg/H, Si/H, Ca/H, Sc/H, Ti/H, Cr/H, Mn/H, Fe/H and Ni/H ratios for four A-F stars.

It should be noted that the gaseous O/H values derived from H II regions with the [O III] (4363/5007) temperature are about 0.25 dex smaller than the stellar values. After the H II values are corrected by the t^2 factor and by the fraction of O atoms trapped in dust, the stellar and the H II region O/H values become similar.

We calculate also the Z values of the supergiant stars, in the same way as for

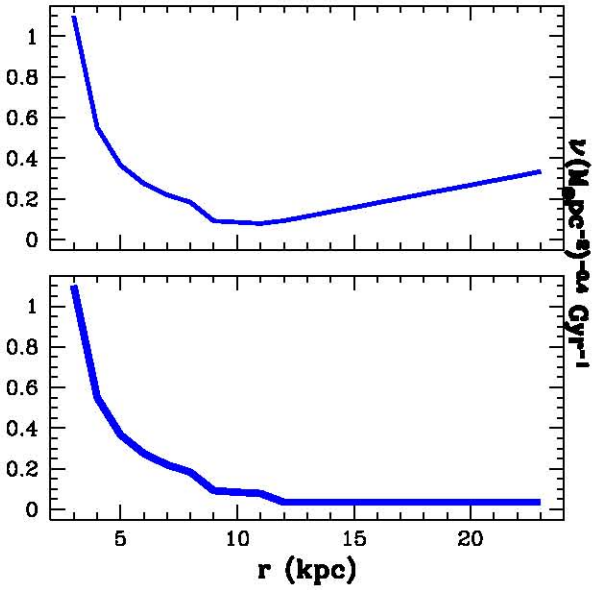

Figura 4.3: Radial distribution of the star formation efficiency, $\nu = SFR/M_{gas}^{1.4}$, of our CEM. Top panel: for $0 < t(\mathrm{Gyr}) \leq 12.8$ (thin blue line). Bottom panel: for $12.8 < t(\mathrm{Gyr}) \leq 13.0$ (thick blue line).

the H II regions, thus:

$$Z_{stars} = \frac{\Sigma(X_i)_{stars}}{\Sigma(X_i)_{\odot}} Z_{\odot}, \tag{4.6}$$

(see Figure 4.7, bottom panel).

Figure 4.1, bottom panel, shows the O/H ratios from H II regions and from stars, and Figures 4.4 to 4.7 show the chemical abundances for the other fifteen chemical elements and for Z.

4.4. Chemical evolution model, CEM

In this work, we present a chemical evolution model for the M31 disk. The model is built to reproduce the present radial distributions of: the total baryonic mass, the gas mass, and the O/H values obtained from H II regions.

The characteristics of the model are:

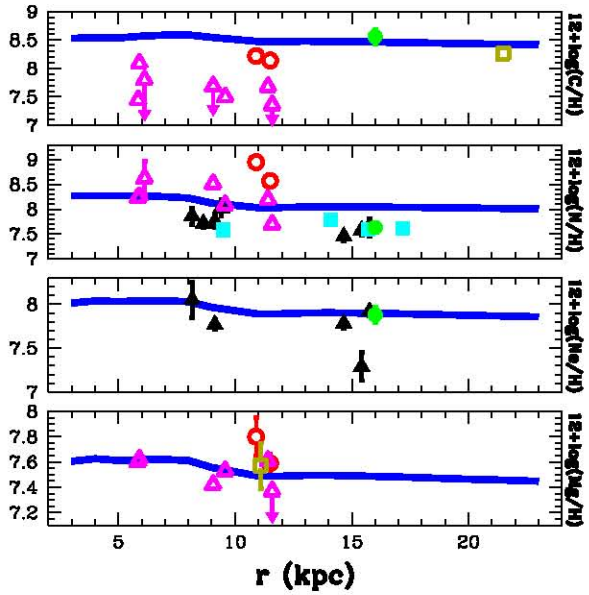

Figura 4.4: Radial distributions at the present time of the C/H, N/H, Ne/H, and Mg/H ratios, CEM (solid blue line). Observational data: (i) gaseous values from H II regions corrected by us for temperature variations (t^2 factor) and dust depletion (see Section 4.3.3), Zurita & Bresolin (2012) (filled black triangles), Sanders et al. (2012) (filled cyan squares), and Esteban et al. (2009) (filled green circle); (ii) stellar values, Przybilla et al. (2006) (empty red circles), Trundle et al. (2002) (empty magenta triangles), and Venn et al. (2000) (empty gold squares). The vertical lines represent one σ errors. Symbols without vertical lines mean abundance ratios without computed errors. Symbols with an arrow represents the upper value of the estimated abundances. The original Ne yields by Kobayashi et al. (2006) are multiplied by 0.6.

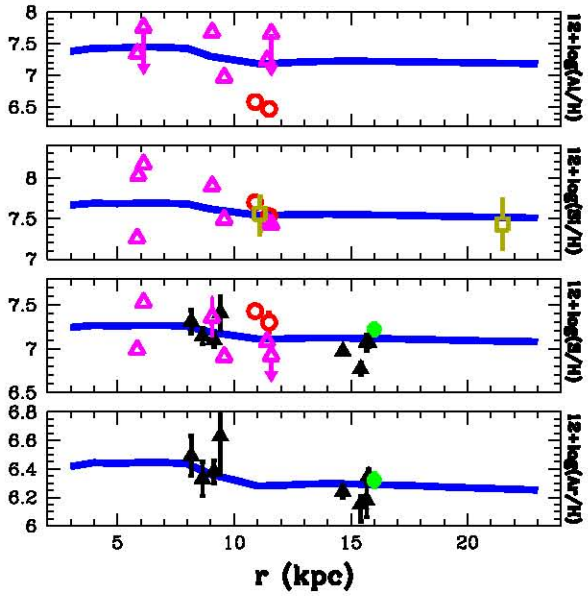

Figura 4.5: Radial distributions at the present time of the Al/H, Si/H, S/H, and Ar/H ratios, CEM (solid blue line). Observational data: symbols and errors as in Fig 4.4. The original Al yields by Kobayashi et al. (2006) are multiplied by 7.

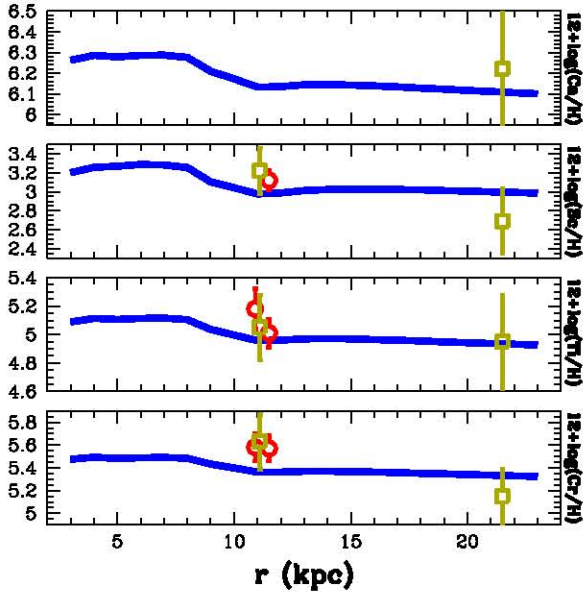

Figura 4.6: Radial distributions at the present time of the Ca/H, Sc/H, Ti/H, and Cr/H ratios, CEM (solid blue line). Observational data: symbols and errors as in Fig 4.4. The original Sc and Ti yields by Kobayashi et al. (2006) are multiplied by 10 and 5, respectively.

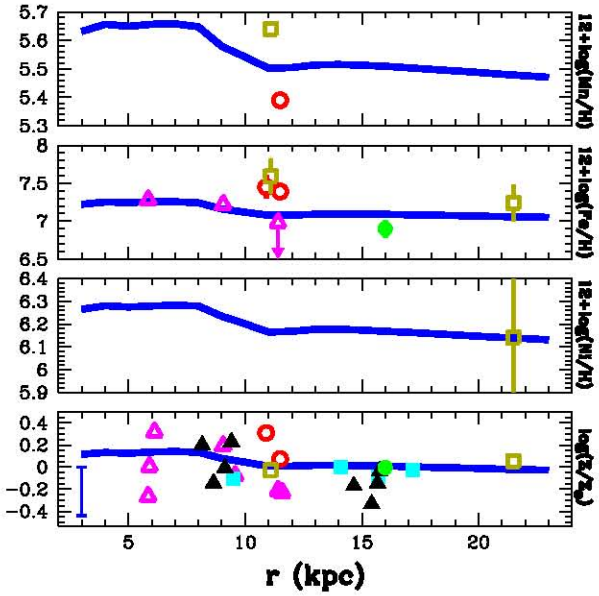

Figura 4.7: Radial distributions at the present time of the Mn/H, Fe/H, Ni/H, and $Z/Z_{\odot}$ ratios, CEM (solid blue line). Observational data: symbols and errors as in Fig 4.4. Only in the bottom panel the vertical blue line in the left corner represents an average error. The original Mn and Ni yields by Kobayashi et al. (2006) are multiplied by 8 and 5, respectively.

i) The halo and disk are projected onto a single disk of negligible width and with azimuthal symmetry; therefore, all the functions are dependent only on the galactocentric distance r and time t. The single disk consists of a series of concentric rings without exchange of matter between them ranging from 3 to 23 kpc and each ring has a width of 1 kpc.

ii) The model describes the $r \geq 3$ kpc region, because the physical processes associated with the bulge and bar in the central region of M31 are not considered.

iii) The age of the model is 13.0 Gyr, the time elapsed since the beginning of the formation of the galaxy to the present time.

iv) The model is built based on an inside-out scenario with a double infall of primordial abundances: $Y_p = 0.2477$, and $Z = 0.00$ (Peimbert et al. 2007). The double-infall rate adopted is similar to that presented by Chiappini, Matteucci & Gratton (1997), is a function of r and t: $IR(r,t) = A(r)e^{-t/\tau_{halo}} + B(r)e^{-(t-1Gyr)/\tau_{disk}}$. The halo formation occurs during the first Gyr with a timescale formation $\tau_{halo} = 0.1$ Gyr, and the disk formation takes place from 1 Gyr until 13 Gyr, with a timescale that depends on the radius $\tau_{disk} = 0.3r(kpc) - 0.2$ Gyr. The variables $A(r) = 48e^{-(r/5.7kpc)}$ and $B(r) = 192e^{-(r/5.7kpc)}$ are chosen to reproduce the present radial distribution of the total baryonic mass in the M31 disk, and we consider that the disk and halo mass distributions match the present mass density of the halo and disk components in the solar neighborhood, $M_{halo}/M_{disk} = 0.25$ (Carigi & Peimbert 2011).

v) The model does not consider the loss of gas and stars from the galaxy to the intergalactic medium, nor gaseous and stellar radial flows through the galactic disk.

vi) The star formation rate SFR was parametrized as the Kennicutt-Schmidt Law (Kennicutt 1998): $SFR(r,t) = \nu(r)M_{gas}(r,t)^n$, with $n = 1.4$. Here ν is the star formation efficiency obtained by adjusting the current gas mass radial distribution.

vii) The model uses the initial mass function (IMF) proposed by Kroupa, Tout & Gilmore (1993), in the mass interval given by 0.08 $M_\odot$ to an upper mass, m_{up}, which is chosen to be 45 $M_\odot$ to reproduce the current absolute value of the O/H gradient of the M31 disk.

viii) Stars pollute the interstellar medium according to a matrix computed by Robles-Valdez, Carigi & Peimbert (2013) from metal-dependent yields of massive stars (MS; $8 < m/M_\odot \leq m_{up}$), low and intermediate mass stars (LIMS; $0.08 \leq m/M_\odot \leq 8$), and Type Ia SNe. For details see their section 4.

4.5. Results and discussion

Given the constraints adopted by us our model is the best one we were able to compute. It is not unique in the sense that in the future the observational data and the yields could be improved, moreover it is likely that in the future additional information might help to construct a better model.

As Figure 4.1 shows, our chemical evolution model reproduces very well $M_{gas}(r)$ and O/H(r) at the present time and for all galactocentric distances. Since for M31 the number of model free parameters and the number of the reliable observational constraints are similar, with only one reasonable combination of the CEM ingredients, the model can match the main observational constraints. Therefore, given an infall, the behavior of the M_{gas} depends mainly on the chosen SFR, and consequently in this work, on the efficiency of star formation for each r, $\nu(r)$. Moreover, the slope of the radial distribution of O/H depends mostly on the infall and the SFR, but the absolute value of O/H(r) is determined by the chosen IMF and its m_{up}, when a chemical yield set is assumed. For all the models that we have built it was necessary to adopt a pronounced scenario inside-out of galactic formation (inner parts are formed much faster than the outer parts) in order to reproduce the observed low M_{gas} and high O/H values for $r < 8$ kpc. The pronounced inside-out scenario of the formation of M31 will be studied in a future article.

We tested several models, nevertheless they were not successful to reproduce the observations at $t = 13$ Gyr. We comment on the main failures of these three models. I) By assuming different values for gas mass thresholds for star formation higher than 4 $M_\odot$ pc^{-2}, it was possible to reproduce reasonably well the radial profile of the M_{gas}, but not the rest of the observables. Particularly, the theoretical chemical abundances were very low, due to the low number of formed stars. Adopting thresholds lower than 4 $M_\odot$ pc^{-2}, the predicted values of the M_{gas} were higher that the observations for $r < 9$ kpc and for $r >12$ kpc. II) By considering a constant ν and $n = 1.4$ in the star formation rate (see Section 3.vi), the predicted M_{gas} profile was a simple exponential, inconsistent with the observational profile. III) By adopting a constant ν and an r-dependent n in the SFR (between $n = 1$ to 2), the theoretical M_{gas} adjusted moderately well the observations, but the models did not reproduce the chemical abundances.

To construct our successful model, we built a CEM with a ν variable in space to reproduce the current M_{gas} for all radii. In Figure 3 (upper panel) we show the radial distribution of the star formation efficiency, for $0.0 < t$(Gyr)< 12.8, which follows the equations: $\nu \sim 4.32/r - 0.34$ for the inner disk, $\nu \sim -0.04r + 0.55$ for the central disk, and $\nu \sim 0.02r - 0.15$ for the outer disk. The r-behavior of

the SFR efficiency can be caused by various physical conditions in the gas of the M31 disk, as distribution and temperature of the molecular gas, processes of turbulence, among others (Leroy et al 2008,. Zamora-Avilés & Semadeni 2013). As is well known, the cause, and therefore the evolution of the *SFR* is still an open problem in astronomy.

With these $\nu(r)$ values (constant in time) the model does not matches the estimated SFR for $r > 12$ kpc, because the observed SFR decreases considerably in this outer zone. Therefore, the model requieres to diminish $\nu(r)$ to a near zero value, only for $r > 12$ kpc and at very recent times, to keep the agreement with $M_{gas}(r)$ and O/H(r). We decided to reduce $\nu(r)$ for $12.8 < t$(Gyr)< 13.0 (see Figure 3, lower panel) based on the results by Block et al. (2006). They, using numerical simulations, explain the ring-like structure observed in the M31 disk at ∼10 kpc as due to a 0.2 Gyr-ago encounter with a companion galaxy (probably M32), and they find that the expected motions around of the ring when the intruder has less mass that of the galactic disk, aparently are different that when the intruder has a larger mass, then, is possible, to be produce a reduction in the gas mass density beyond of the ring, therefore a reduction of the star formation efficiency. With this ν reduction, the model reproduces the outer observed *SFR* and keeps the excellent agreement with other observational constraints (see Figures 4.1 and 4.2).

The theoretical chemical abundance gradients are in good agreement with the abundance determinations from H II regions and supergiant stars (see Figures 4.1, 4.4, 4.5, 4.6 and 4.7). In particular, the predicted C/H values fit well with two C/H determinations from K932 H II region (E09) and from the outermost A-F star (Venn et al. 2000). However, our C/H predictions are higher than most of the C/H stellar values, in particular those by Trundle et al. 2002 (see Figure 4.4, upper panel). In order to explain the observational differences, it is necessary to determine stellar C abundances with higher precision.

All the predicted Xi/H gradients, at the present time, show three slopes (see Figures 4.1 and 4.4-4.7): slightly positive for $3 < r$(kpc)< 8 (inner disk), negative for $8 < r$(kpc)< 11 (central disk), and slightly negative for $11 < r$(kpc)< 23 (outer disk). As we previously mentioned, in these regions $\nu(r)$ presents three different behaviors for the most of the evolution (see Figure 4.3, upper panel). Therefore, the different gradients are mainly due to the radial variations of ν.

Outside of the Local Group, both radial flattening in the chemical gradients has been observed in spiral galaxies in the outermost radii (Vlajić 2010; Goddard et al. 2011; Bresolin, Kennicutt & Ryan-Weber 2012), and in the innermost radii (Rosales-Ortega et al. 2011; Sanchéz et al. 2013). Nevertheless, in the Local Group the flattening has been observed only in the outer zone if the Milky Way (see

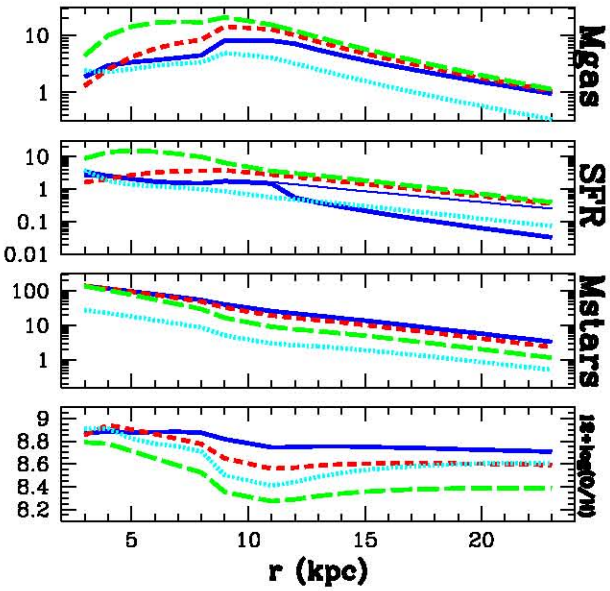

Figura 4.8: Radial distributions of: M_{gas} ($M_\odot pc^{-2}$), SFR ($M_\odot pc^{-2} Gyr^{-1}$), M_{stars} ($M_\odot pc^{-2}$), and O/H abundances for our CEM at four times: 1, 4, 8 and 13 Gyr (dotted cyan, long-dashed green, short-dashed red and solid blue lines, respectively). Only for the SFR the r-behavior at $t = 12.8$ Gyr is shown (thin blue line).

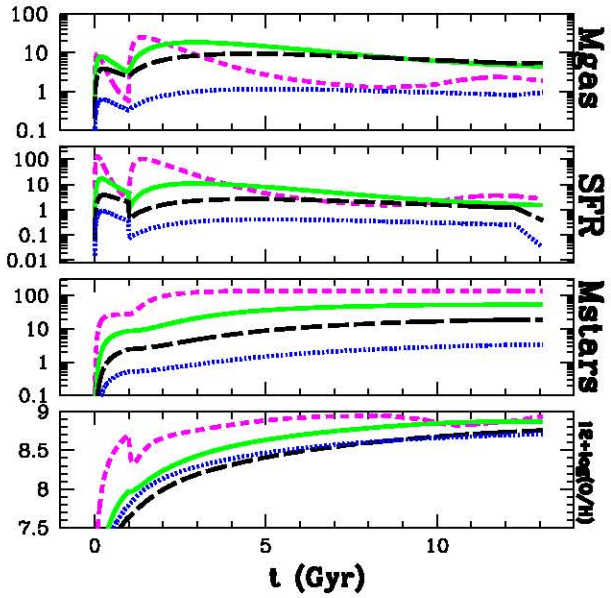

Figura 4.9: Evolution of: M_{gas}, SFR, M_{stars}, and O/H abundances for our CEM at four radii: 3, 8, 13, and 23 kpc (short-dashed magenta, solid green, long-dashed black, and dotted blue lines, respectively).

Esteban et al. 2013, and references therein). Esteban et al. build a CEM, in which they increased the ν values for $r > 10$ kpc $\sim R_{25}^{MW}$, in order to reproduce the outer flattened gradients in the MW. The increase did not affect the agreement with other observational constraints of the MW. Similarly in our CEM, ν is increased for $r >$ 12 kpc $\sim$ 1/2 R_{25}^{M31}, in order to reproduce the M_{gas}, and under this assumption, the model adjusts very well the chemical abundances determined in the outermost H II region and the outermost A-F supergiant star. Given the paucity of data in the inner and outer regions, it is necessary to obtain more and better observations, in order to confirm that the chemical gradients in the inner and outer parts of the Andromeda galaxy are flat.

When we consider the original Ne, Al, Sc, Ti, Mn, and Ni yields by Kobayashi et al. (2006), our model does not agree with the observed chemical abundances of these elements. Therefore, we have to multiply these yields by 0.6, 7.0, 10.0, 5.0, 8.0, and 5.0, respectively, in order to improve the agreement. Previous authors also applied corrections to the original yields computed by Kobayashi et al., e.g.: Hernández-Martínez et al. (2011) estimated that the original Cl and Ar should be multiplied by 6 and 2, respectively, to adjust the Cl/H and Ar/H gradients from H II regions, and young and old planetary nebulae in the dwarf irregular galaxy NGC 6822. Cescutti et al. (2012) multiplied the original P yield by 3 to match the P/H gradient from stars in the Milky Way disk. Robles-Valdez et al. (2013) multiplied the original Ar yield by 2 to reproduce the Ar/H gradient from H II regions in the M33 disk.

In this work we think that it is plausible to modify the stellar yields of these specific elements, because the agreement of the chemical evolution models by Kobayashi et al. (2006, 2011), using their own yields, were not so good for Sc/Fe, Ti/Fe, Mn/Fe, and Ni/Fe ratios. For Ne/Fe, they could not compare their model results, due to the lack of data. It is important to mention that Kobayashi et al. took into account only stellar abundances as observational constraints and that the line intensities of those elements are very weak in the stellar spectrum, hindering the determination of those abundances. Therefore, the chemical abundances from H II regions, together with a CEM, can provide strong constraints on stellar evolution models.

In Figure 4.8, we show the radial distributions of: M_{gas}, SFR, M_{stars}, and O/H abundances at four times: 1, 4, 8, and 13 Gyr. Only for the SFR plot, we add the predicted values at 12.8 Gyr (see thin blue line) to compare with the 13-Gyr values, in order to show the effect of the ν reduction during the last 0.2 Gyr. Between 1 and 4 Gyr, M_{gas} increases and O/H decreases due to the enormous amount of primordial gas that falls to form the disk, and the SFR increases as M_{gas} because

the SFR is proportional to the $M_{gas}^{1.4}$. Between 4 and 13 Gyr, and mostly in the very inner radii, the decline of the infall causes the decrease of M_{gas} and consequently the reduction of the SFR, although the ν is higher. Since the M_{stars} is a time-accumulative process of the SFR, M_{stars} always increases with time.

In the lower panel of Figure 4.8, the radial distribution of O/H shows three gradients that flatten at different rates, during the evolution. The differences in the flattening rates are due to the changes in the O enrichment and the H dilution. The O enrichment depends on the SFR through the adopted ν values, and the H dilution depends on the infall rate predicted by the inside-out scenario. For $r < 8$ kpc, the original negative gradient, produced by a higher SFR to infall ratio in the inner radii, becomes slightly positive, because the SFR is more important at the central radii than at the inner radii during the last half of the evolution. For $8 < r$ (kpc) < 11 kpc, the flattening with time is less pronounced than that for the inner region, because ν is not so r-dependent, and the gradient evolution is dominated by the infall rate. For $r > 11$ kpc, the original positive gradient, produced by a higher SFR to infall rate in the outer radii, becomes slightly negative, due to the gas dilution in the outer radii at recent times.

In Figure 4.9, we present the evolution of: M_{gas}, SFR, M_{stars}, and O/H values at four radii: 3, 8, 13 and 23 kpc. For $r = 3$ kpc and at early times, the values of these properties are higher than those for outer radii, due to the large quantity of material accreted into the inner radii compared to the outermost parts (inside-out scenario, see Figure 4.10, right panel). For $r = 3$ kpc and $t > 10$ Gyr, M_{gas} increases due to the bulk of very-low-mass stars (VLMS) that formed during the first 3 Gyrs and that died recently, ejecting as a whole, huge amounts of gas to the interstellar medium. Since the expelled material by these VLMS is composed mainly by hydrogen and helium, the dying stars dilute the interstellar medium in heavy elements, and consequently O/H decreases. For the outermost radii and $t >$ 12.8 Gyr, the SFR diminishes due to the reduction of the star formation efficiency, necessary to reproduce the observed SFR. As mentioned before, M_{stars} increases with time for all radii (see Figure 4.8), but that increase is different for each radii at a given time (see Figure 4.9). For inner radii, the increase rate of M_{stars} is higher at early times, on the contrary for outer radii, the increase rate is higher at recent times. This behavior is consequence of the inside-out scenario.

In Figure 4.10 we present the radial distribution of infall at eight times: 1, 2, 3, and 4 Gyr (left-top panel), and 6, 8, 11, and 13 Gyr (left-bottom panel). In the right panel, we show the evolution of infall at four radii: 3, 8, 13, and 23 kpc. It can be noted that this infall rate produces a more pronounced inside-out galactic formation than that of the Milky Way (Carigi & Peimbert 2011) and that of the

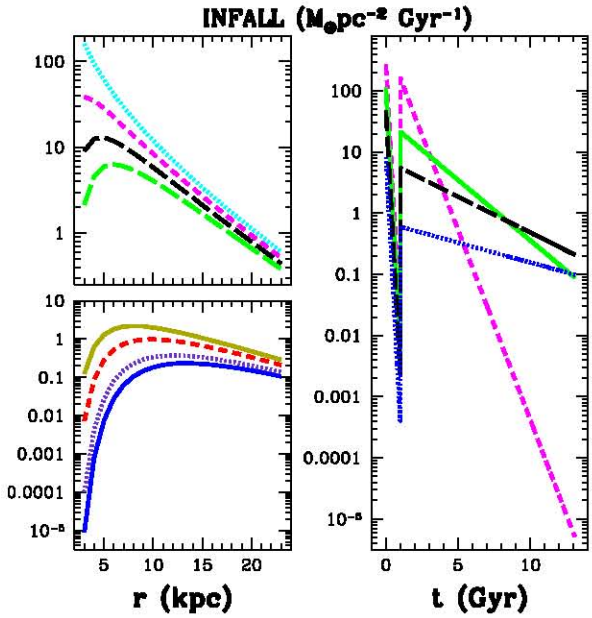

Figura 4.10: Infall rate for our CEM. Left top panel: radial distribution at four times: 1, 2, 3 and 4 Gyr (dotted cyan, short-dashed magenta, long-dashed black and long-dashed green lines, respectively). Left bottom panel: radial distribution at four times: 6, 8, 11 and 13 Gyr (solid gold, short-dashed red, dotted violet, and solid blue lines, respectively). Right panel: Evolution at four radii: 3, 8, 13, and 23 kpc (short-dashed magenta, solid green, long-dashed black, and dotted blue lines, respectively).

M33 (Robles-Valdez et al. 2013). At early times, the accretion in our M31 model is much more intense in the inner regions; but at recent times, the accretion is more important in the outer regions compared to the infall rate inferred for the MW and M33.

4.6. The helium and oxygen enrichment in M31

In Figure 4.11, we present the evolution of ΔY vs ΔO and $\Delta Y/\Delta O$ ratio obtained from our CEM for r = 15 kpc. In general the values of ΔY and ΔO increase with the evolution, but in the Figure 4.11 (top panel) presents a decrease in the values, caused by the dilution of interstellar medium, due to the huge amount of

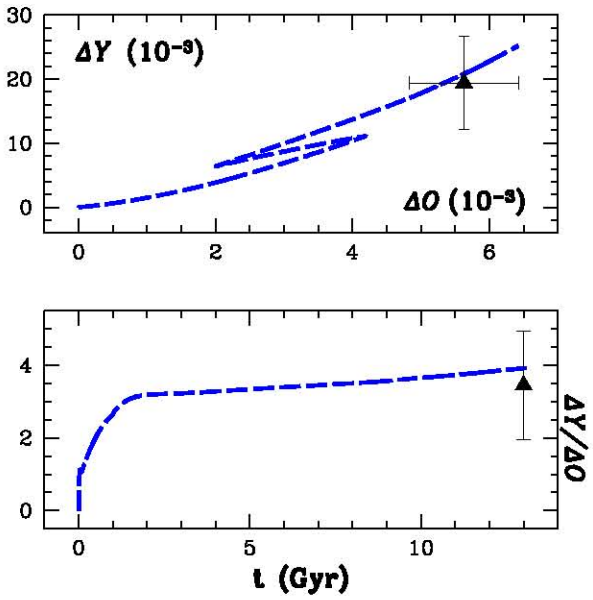

Figura 4.11: Results of CEM at $r = 15.0$ kpc (dashed-blue line). Top panel: ΔY versus ΔO evolution. Bottom panel: $\Delta Y/\Delta O$ evolution. Observational data at $r = 14.7$ kpc: oxygen value obtained from the O/H gradient (see equation 4.4 in Section 4.3.3), and helium value derived in Section 4.6.

primordial gas accreted at the beginning of the second infall. In the bottom panel, the model shows an important increase of the $\Delta Y/\Delta O$ ratio for $t < 1.5$ Gyr, because the most massive stars pollute the interstellar medium with more helium than oxygen, then the LIMS pollute with helium and do not produce oxygen.

Moreover, we compare the theoretical values at 13 Gyr with observed values for $r = 14.7$ kpc. ΔY is the helium mass fraction produced after the primordial nucleosyntesis and it is obtained from the Y value of an H II region minus the primordial helium abundance, Y_p. On the other hand, ΔO is the oxygen mass fraction in a given H II region. The study of the $\Delta Y/\Delta O$ ratio is important to check the consistency of the chemical evolution model since He is produced by LIMS and MS, while O is mainly produced by MS. For this reason the $\Delta Y/\Delta O$ ratio depends on: i) the IMF, because it gives the ratio between the number of LIMS and MS; ii) the SFR, because it provides the total stellar mass; iii) the stellar lifetimes, because they are equivalent to the time delays between the star formation and the contribution of LIMS and MS to the ISM enrichment; iv) the He and O yields, because they represent the stellar efficiency of producing He and O; and v) gas flows in and out of the considered values.

There are two H II regions of M31 with the best He/H determinations in the literature, objects 25 and 26 by Zurita & Bresolin (2012), both regions at a galactocentric distance of 14.7 kpc. These authors derived He^+/H^+ values of 0.086±0.004 and 0.088±0.005 for regions 25 and 26 respectively, based on the He atomic data by Porter et al. (2005, 2007).

Based on the He I and H I emission lines by Zurita & Bresolin (2012), we use the program by Peimbert et al. (2012) with the He I atomic data by Porter et al. (2013) and derive values of He^+/H^+ of 0.0792 and 0.0839 for objects 25 and 26, respectively. To correct for the presence of neutral helium we assume that He^0/He=S^+/S, and based on the S^+/S ratios presented by Zurita & Bresolin (2012), obtain values of He/H of 0.0876±0.0050 and 0.0981±0.0050 for regions 25 and 26. Therefore, for $r = 14.7$ kpc, we adopt a value of He/H=0.0928±0.0035, the average of both determinations.

For a galactocentric distance of 14.7 kpc and based on the O/H gradient (see equation 4) we obtain that 12 + log(O/H) = 8.70 ± 0.06. Under the assumption that O amounts to 42 % of the total Z value (Peimbert et al. 2007b) it follows that $X = 0.7195 \pm 0.0074$, $Y = 0.2671 \pm 0.0073$ and $Z = 0.0134 \pm 0.0020$.

From the X, Y and Z values we obtain an O by mass of 0.00563 ± 0.0008, and a $\Delta Y = 0.0194 \pm 0.0079$, consequently $\Delta Y/\Delta O = 3.45 \pm 1.50$. As in our previous works, we have adopted the Y_p value by Peimbert et al. (2007a) of 0.2477 ± 0.0029. This Y_p value is in very good agreement with the Planck satellite predic-

tion of Y_p, in standard Big Bang nucleosynthesis, that amounts to 0.2473 ± 0.0003 (Ade et al. 2013).

4.7. Conclusions

We reach the following conclusions:

(1) The O/H abundance ratios from A, B and A-F supergiant stars agree with the abundances derived from H II regions only if the gaseous abundances determined from recombination lines are corrected by dust depletion. Moreover, the stellar O/H values agree with the O/H gaseous values derived from collisional excitation lines only if they are increased by the effect of temperature variations and by the fraction of O atoms embedded in dust grains.

(2) After correcting the O/H abundances from H II regions by t^2 and dust depletion, the O/H gradient in the 7-18 kpc region is well represented by:

$$12 + \log(\mathrm{O/H}) = (8.73 \pm 0.06) - (r - 12)(0.013 \pm 0.006).$$

(3) An upper mass in the IMF for M31 equal to 45 $M_\odot$ is required to reproduce the absolute value of the observed O/H gradient.

(4) The original yields of Ne, Al, Sc, Ti, Mn and Ni computed by Kobayashi et al. (2006) have to be multiplied by 0.6, 7, 10, 5, 8 and 5, in order to reproduce the absolute value of the Ne/H, Al/H, Sc/H, Ti/H, Mn/H and Ni/H gradients, respectively.

(5) The $\Delta Y/\Delta O$ value determined from observations is in agreement with the model.

(6) M31 has been formed according to a pronounced inside-out scenario. This fact is necessary to reproduce the low values of M_{gas} in the inner radii of the disk.

(7) A star formation efficiency, $\nu(r)$, variable in space and constant in time for most of the evolution is necessary to reproduce the current profile of the gas mass density for whole galactic disk.

(8) A considerable reduction of the ν value, for $t > 12.8$ Gyr and for $r > 12$ kpc is inferred to explain the important decrease of the *SFR* observed in the outer regions.

9) Each predicted Xi/H gradient shows three slopes during the whole evolution, due to the three r-behaviours of ν. These slopes flatten at different rates, due to the combination of $\nu(r)$ and the infall rate that depends on r and t, according to the inside-out scenario. For the inner and outer part the current gradients are slightly positive, while in the central part the slope is slightly negative. More

and better determinations of chemical abundances are required to confirm these results.

Bibliografía

Ade P., Aghanim N., Armitage-Caplan C., Arnaud M., Ashdown M., Atrio-Barandela F., Aumont J., et al, 2013, in press, (arXiv:1303.5076)

Asplund M., Grevesse N., Sauval A., Scott P., 2009, ARAA, 47, 481

Barmby P., Ashby M., Bianchi L., Engelbracht C., Gehrz R., Gordon K., Hinz, J., et al., 2006, ApJ, 650, L45

Berkhuijsen E., 1977, A&A, 57, 9

Blair W., Kirshner R., Chevalier R., 1982, ApJ, 254, 50

Block D., Bournaud F., Combes F., Groess R., Barmby P., Ashby M., Fazio G., Pahre M., Willner S., 2006, Nature, 443, 832

Boissier S., Prantzos N., Boselli A., Gavazzi G., 2003, MNRAS, 346, 1215

Boissier S., Gil de Paz A., Boselli A., Madore B., Buat V., Cortese L., Burgarella D., et al., 2007, ApJS, 173, 524

Braun R., 1991, ApJ, 372, 54

Braun R., Thilker D., Walterbos R., Corbelli E., 2009, ApJ, 695, 937

Bresolin F., Kennicutt R., Ryan-Weber E., 2012, ApJ, 750, 122

Carigi L., García-Rojas J., Meneses-Goytia S., 2013, RMxAA, 49, 253

Carigi L., Peimbert M., 2008, RMxAA, 44, 341

Carigi L., Peimbert M., 2011, RMxAA, 47, 139

Cescutti G., Matteucci F., Caffau E., Francois P., 2012, A&A, 540, 33

Chemin L., Carigman C., Foster T., 2009, ApJ, 705, 1395

Croxall K., Smith J., Brandl B., Groves B., Kennicutt R., Kreckel K., Johnson B., et al., 2013, ApJ, 777, 96

Dame T., 1993, Back to the Galaxy, New York: Springer, 267

Dame T., Koper E., Israel F., Thaddeus P., 1993, ApJ, 418, 730

Dennefeld M., Kunth D., 1981, AJ, 86, 989

Fu J., Hou J., Yin J., 2009, ApJ, 696, 668

Esteban C., Bresolin F., Peimbert M., García-Rojas J., Peimbert A., Mesa-Delgado A., 2009, ApJ, 700, 654 (E09)

Esteban C., Carigi L., Copetti M., García-Rojas J., Mesa-Delgado A., Castañeda H., Péquignot D., 2013, MNRAS, 433, 382

Galarza V., Walterbos R., Braun R., 1999, AJ, 118, 2775

Goddard Q., Bresolin F., Kennicutt R., Ryan-Weber E., Rosales-Ortega F., 2011, MNRAS, 412, 1246

Hernández-Martínez L., Carigi L., Peña M., Peimbert M., 2011, A&A, 535, 118

Hiromoto N., Maihara T., Oda N., Okuda H., 1983, PASJ, 35, 41

Kennicutt R., 1998, ApJ, 498, 541

Kennicutt R., Evans N., 2012, ARAA, 50, 531

Kobayashi C., Umeda H., Nomoto K., Tominaga N., Ohkubo T., 2006, ApJ, 653, 1145

Kobayashi C., Karakas A., Umeda H., 2011, MNRAS, 414, 3231

Koper E., Israel F., Dame T., Thaddeus P., 1991, AJ, 383, L11

Kroupa P., Tout C., Gilmore G., 1993, MNRAS, 262, 545

Leroy A., Walter F., Brinks E., Bigiel F., de Blok W., Madore B., Thornley M., 2008, AJ, 136, 2782

Loinard L., Dame T., Heyer M., Lequeux J., Thaddeus P., 1999, A&A, 351, 1087

Marcon-Uchida M., Matteucci F., Costa R., 2010, A&A, 520, A35

Mattsson L., 2008, Physica Scripta, 133, 014027

Mesa-Delgado A., Esteban C., García-Rojas J., Luridiana V., Bautista M., Rodríguez M., López-Martín L., Peimbert M., 2009, MNRAS, 395, 855

Nieten Ch., et al., 2006, A&A, 453, 459

Pilyugin L., Vilchez J., Contini T., 2004, A&A, 425, 849

Peimbert A., Peimbert M., 2010, ApJ, 724, 791

Peimbert A., Peña-Guerrero M., Peimbert M., 2012, ApJ, 753, 39

Peimbert M., 1967, ApJ, 150, 825

Peimbert M., Luridiana V., Peimbert A., 2007a, ApJ, 666, 636

Peimbert M., Luridiana V., Peimbert A., Carigi L., 2007b, ASPC, 374, 81

Peña-Guerrero M., Peimbert A., Peimbert M., 2012, ApJ, 756L, 14

Porter R. L., Bauman R. P., Ferland G. J., MacAdam K. B., 2005, ApJ, 622, L73

Porter R. L., Ferland G. J., MacAdam K. B., 2007, ApJ, 657, 327

Porter R., Ferland G., Storey P., Detisch M., 2013, MNRAS, 433L, 89

Prantzos N., Aubert O., 1995, A&A, 302, 69

Przybilla N, Butler K., Kudritzky R., 2006, preprint conference proceeding, (arXiv:0611.044)

Renda A., Kawata D., Fenner Y., Gibson B., 2005, MNRAS, 356, 1071

Robles-Valdez F., Carigi L., Peimbert M., 2013, MNRAS, 429, 2351

Rosales-Ortega F., Díaz A., Kennicutt R., Sánchez S., 2011, MNRAS, 415, 2439

Sánchez S., Rosales-Ortega F., Páramo-Iglesias J., et al., 2013, A&A submitted, arXiv:1311:7052

Sanders N., Caldwell N., McDowell J., Harding P., 2012, ApJ, 758, 133S

Scalo J., 1986, Fund. Cosm. Phys., 11, 1

Spitoni E., Recchi S., Matteucci F., 2008, A&A, 484, 743

Spitoni E., Matteucci F., 2011, A&A, 531, A72

Spitoni E., Matteucci F., Marcon-Uchida M., 2013, A&A, 551, 123

Tabatabaei F., Berkhuijsen E., 2010, A&A, 517, A77

Tamm A., Tempel E., Tenjes P., Tihhonova O., Tuvikene T., 2012, A&A, 546, 4

Trundle C., Dufton P., Lennon D., Smartt S., Urbaneja M., 2002, A&A, 395, 519

Venn K., McCarthy J., Lennon D., Przybilla N., Kudritzki R., Lemke M., 2000, ApJ, 541, 610

Villardel F., Ribas I., Jordi C., Fitzpatrick E., Guinan E., 2010, A&A, 509, A70

Vlajić M., 2010, PASA, 27, 252

Walterbos R., 1986, BAAS, 18, 915

Walterbos R., Kennicutt A., 1988, A&A, 198, 61

Widrow L., Perrett K., Suyu S., 2003, ApJ, 588, 311

Williams B., 2003a, AJ, 126, 1312

Williams B., 2003b, MNRAS, 340, 143

Worthey G., España A., McArthur L., Courteau S., 2005, ApJ, 631, 820

Wyse R., Silk J. 1989, ApJ, 339, 700

Yin J., Hou J., Prantzos N., Boissier S., Chang R., Shen S., Zhang B., 2009, A&A, 505, 497

Zamora-Avilés M., Vázquez-Semadeni E., 2013, submitted ApJ

Zurita A., Bresolin F., 2012, MNRAS, 427, 1463